EXACT NEURAL FIELDS INCORPORATING GAP JUNCTIONS

CARLO R. LAING

Abstract. We consider networks of quadratic integrate-and-fire neurons coupled via both chemical synapses and gap junctions. After transforming to "theta neuron" coordinates, a network's governing equations are of a form amenable to the use of the Ott/Antonsen ansatz. This ansatz allows us to derive an exact description of a network's dynamics in the limit of an infinite number of neurons. For an all-to-all connected network we derive a single (complex) ordinary differential equation while for spatially extended networks we derive neural field equations (nonlocal partial differential equations). We perform extensive numerical analysis of the resulting equations, showing how the presence of gap junctional coupling can destroy certain spatiotemporal patterns such as stationary "bump" solutions and create others such as travelling waves and spatiotemporal chaos. Our results provide significant insight into the effects of gap junctions on the dynamics of networks of Type I neurons.

1. Introduction

Neural field models have been used for many years to understand largescale spatiotemporal dynamics of the brain [9, 13, 20, 15, 2]. Specific applications include neurophysiological phenomena such as working memory [44], binocular rivalry [11], orientation tuning in the visual cortex [4], the head direction system [66] and EEG rhythms [62]. The models normally take the form of nonlocal differential equations, where the nonlocality arises from long distance synaptic connections between different parts of the cortex. The dynamic variables in such models are normally referred to as "average somatic voltage" or "synaptic drive", but despite this the derivation of a neural field model from a particular network of individual neurons is often not discussed. When such derivations are performed they normally rely on a number of assumptions such as a separation of timescales between neuron and synaptic dynamics [9, 20].

Almost all neural field models studied so far have included synaptic connections but have ignored the other common form of connectivity, namely gap junctions [6, 26]. At the

Date: June 29, 2015.

2000 *Mathematics Subject Classification.* 92C20, 34C15, 37G35, 34D06, 35B36.

Key words and phrases. neural field, quadratic integrate-and-fire, gap junction, Ott/Antonsen, bifurcation, theta neuron.

simplest level of description, gap junctions act by allowing a current to flow between two connected neurons in direct proportion to the difference in voltages of the two neurons (the current flows from high voltage to low voltage). Many authors have investigated the effects of gap junctional coupling between model neurons, [14, 18, 12, 22, 32] often using the assumption of weak coupling [29, 56]. Many of these studies have been for pairs of neurons rather than networks [3, 47, 60, 30].

In this paper we give an exact derivation of neural field models for networks of quadratic integrate-and-fire neurons, coupled through both synapses and gap junctions, thus resolving (at least partially) the issues mentioned above. The models are exact in the limit as the number of neurons goes to infinity, but we find that they predict well the behaviour of large networks of individual neurons. Note that the derivations do not rely on coupling being weak. Fully understanding all possible effects of gap junctional coupling is clearly a huge undertaking, so here we focus on a small number of representative scenarios.

Our work builds primarily on the results of Ermentrout on gap junction coupled noisy theta neurons [22], Luke et al.'s success in applying the Ott/Antonsen ansatz to networks of theta neurons [48], similar work by Montbrió et al. on quadratic integrate-and-fire neurons [50], and the work of Laing [42]. The structure of the paper is as follows. We consider all-to-all connected networks in Sec. 2, with both excitatory and inhibitory synaptic coupling. In Sec. 3 we consider several one-dimensional networks of neurons with spatially-structured coupling, one with Mexican-hat type coupling which supports "bump" solutions, and one with purely excitatory coupling for which front solutions exist. In Sec. 4 we study two-dimensional networks, but for brevity only consider circularly-symmetric solutions. We conclude in Sec. 5.

2. All-to-all connectivity

Consider a network of N quadratic integrate-and-fire (QIF) neurons [46, 28], all-to-all coupled via both synapses (which act by injecting currents into the neurons) and gap junctions. Such neurons are canonical models for Type I neurons for which the onset of firing is through a saddle-node on an invariant circle bifurcation [21]. Initially ignoring synaptic coupling, the equations are

$$\frac{dV_j}{dt} = I_j + V_j^2 + \frac{g}{N}\sum_{k=1}^{N}(V_k - V_j) \tag{1}$$

for $j = 1, 2, \ldots N$, with the rule that if $V_j(t^-) = \infty$ then $V_j(t^+) = -\infty$. I_j is the current injected into the jth neuron when all of them are uncoupled, and g is the strength of

gap junction coupling. First, rewrite (1) as

$$\frac{dV_j}{dt} = I_j + V_j^2 - gV_j + \frac{g}{N}\sum_{k=1}^{N} V_k. \tag{2}$$

Now let $V_j = \tan(\theta_j/2)$ (the standard transformation to the "theta neuron" [24]). Then

$$\frac{dV_j}{dt} = \frac{d\theta_j/dt}{2\cos^2(\theta_j/2)} = I_j + \tan^2(\theta_j/2) - g\tan(\theta_j/2) + \frac{g}{N}\sum_{k=1}^{N}\tan(\theta_k/2) \tag{3}$$

so

$$\frac{d\theta_j}{dt} = 1 - \cos\theta_j + (1+\cos\theta_j)\left[I_j - g\tan(\theta_j/2) + \frac{g}{N}\sum_{k=1}^{N}\tan(\theta_k/2)\right] \tag{4}$$

Noting that

$$\tan(\theta/2) = \frac{\sin\theta}{1+\cos\theta} \tag{5}$$

we have

$$\frac{d\theta_j}{dt} = 1 - \cos\theta_j - g\sin\theta_j + (1+\cos\theta_j)\left[I_j + \frac{g}{N}\sum_{k=1}^{N}\tan(\theta_k/2)\right] \tag{6}$$

When a neuron fires, at $\theta = \pi$, the term involving tan becomes infinite. To avoid this problem we follow [22] and replace $\tan(\theta/2)$ in (6) by

$$q(\theta) \equiv \frac{\sin\theta}{1+\cos\theta+\epsilon} \tag{7}$$

where $0 < \epsilon \ll 1$, thereby removing the singularity.

We now add synaptic coupling to the model, following [22]. Our full model is

$$\frac{d\theta_j}{dt} = 1 - \cos\theta_j - g\sin\theta_j + (1+\cos\theta_j)\left[I_j + \frac{g}{N}\sum_{k=1}^{N} q(\theta_k) + \kappa\bar{s}\right] \tag{8}$$

where κ is the strength of synaptic coupling and

$$\bar{s} = \frac{1}{N}\sum_{k=1}^{N} s_k, \tag{9}$$

where each s_k satisfies

$$\tau\frac{ds_k}{dt} = a_n(1-\cos\theta_k)^n - s_k; \qquad n \in \mathbb{N}^+ \tag{10}$$

and a_n is chosen so that

$$\int_0^{2\pi} a_n(1-\cos\theta)^n d\theta = 2\pi \tag{11}$$

i.e. $a_n = 2^n(n!)^2/(2n)!$. Setting $\tau = 0$ we recover the instantaneous synapses of [48].

We assume that the I_j are randomly chosen from a distribution $h(I)$ and take the continuum limit, $N \to \infty$. The system is then described by the probability density function $F(I,\theta,t)$ which satisfies [51, 64, 1]

$$\frac{\partial F}{\partial t} + \frac{\partial}{\partial \theta}(Fv) = 0 \tag{12}$$

where

$$v(I,\theta,t) \equiv 1 - \cos\theta - g\sin\theta + (1+\cos\theta)\left[I + gQ(t) + \kappa S(t)\right], \tag{13}$$

where

$$Q(t) \equiv \int_{-\infty}^{\infty}\int_0^{2\pi} F(I,\theta,t)q(\theta)\ d\theta\ dI \tag{14}$$

and $S(t)$ satisfies

$$\tau\frac{dS}{dt} = \int_{-\infty}^{\infty}\int_0^{2\pi} F(I,\theta,t)a_n(1-\cos\theta)^n\ d\theta\ dI - S. \tag{15}$$

We also introduce the complex order parameter, as considered by Kuramoto in the context of coupled phase oscillators [33, 64]

$$z(t) \equiv \int_{-\infty}^{\infty}\int_0^{2\pi} F(I,\theta,t)e^{i\theta}\ d\theta\ dI. \tag{16}$$

The form of (13) means that (12) is amenable to the use of the Ott/Antonsen ansatz [54, 53], and thus we write

$$F(I,\theta,t) = \frac{h(I)}{2\pi}\left\{1 + \sum_{j=1}^{\infty}[\alpha(I,t)]^j e^{ji\theta} + \text{c.c.}\right\} \tag{17}$$

for some function α, where "c.c." means the complex conjugate of the previous term. Functions of the form (17) are said to lie on the Ott/Antonsen (OA) manifold and [54, 53] showed that solutions of (12), where v is of a particular form, exponentially decay onto the OA manifold provided the oscillators are not identical. Thus we can determine the asymptotic dynamics of (12) by restricting to the OA manifold. Substituting the ansatz (17) into (16) we have

$$z(t) = \int_{-\infty}^{\infty} h(I)\bar{\alpha}(I,t)\ dI \tag{18}$$

where overbar indicates complex conjugate. If $h(I)$ is the Lorentzian centered at $I = I_0$, with width Δ, i.e.

$$h(I) = \frac{\Delta/\pi}{(I - I_0)^2 + \Delta^2} \tag{19}$$

then $z(t) = \bar{\alpha}(I_0 + i\Delta, t)$ [53]. Repeating calculations from [61, 42] we find that S satisfies

$$\tau \frac{dS}{dt} = H(z(t); n) - S \tag{20}$$

where

$$H(z; n) = a_n \left[C_0 + \sum_{j=1}^{n} C_j (z^j + \bar{z}^j) \right] \tag{21}$$

and

$$C_j = \sum_{k=0}^{n} \sum_{m=0}^{k} \delta_{k-2m,j} P_{kj} \tag{22}$$

and

$$P_{kj} = \frac{n!(-1)^k}{2^k (n-k)! j! (k-j)!} \tag{23}$$

It can be shown that for impulsive coupling, $H(z; \infty) = (1 - |z|^2)/(1 + z + \bar{z} + |z|^2)$. We will set $n = 2$ in all following calculations. We express $q(\theta)$ in the Fourier series

$$q(\theta) = \sum_{m=-\infty}^{\infty} b_m e^{im\theta} \tag{24}$$

where

$$b_m = \frac{1}{2\pi} \int_0^{2\pi} q(\theta) e^{-im\theta} \, d\theta \tag{25}$$

Note that $b_0 = 0$, each b_m is imaginary and that $b_{-m} = \bar{b}_m$. For $m \geq 1$ we have

$$b_m = \frac{i(\rho^{m+1} - \rho^{m-1})}{2(\rho + 1 + \epsilon)} \tag{26}$$

where $\rho \equiv \sqrt{2\epsilon + \epsilon^2} - 1 - \epsilon$. Thus

$$\int_0^{2\pi} F(I, \theta, t) q(\theta) \, d\theta = h(I) \sum_{m=1}^{\infty} (b_m \bar{\alpha}^m + \text{c.c.}) \tag{27}$$

and

$$Q(t) = \sum_{m=1}^{\infty} (b_m z^m + \text{c.c.}) \tag{28}$$

We will set $\epsilon = 0.01$ and truncate (28) after 100 terms in all following calculations. Now from the form of (13) we know [49] that α satisfies

$$\frac{\partial \alpha}{\partial t} = -i\left[\frac{I+gQ+\kappa S-1+ig}{2} + (1+I+gQ+\kappa S)\alpha + \left(\frac{I+gQ+\kappa S-1-ig}{2}\right)\alpha^2\right] \tag{29}$$

and evaluating this at $I = I_0 + i\Delta$ we obtain

$$\frac{dz}{dt} = \frac{(iI_0-\Delta)(1+z)^2 - i(1-z)^2}{2} + \frac{i(1+z)^2(gQ+\kappa S)+g(1-z^2)}{2} \tag{30}$$

The first term in (30) describes the dynamics of the uncoupled network, and the second, the influence of coupling, both synaptic and gap junctional. Equations (30) and (20) exactly describe the dynamics of the network, where Q is given by (28). One physical meaning of $z \in \mathbb{C}$ is as follows: writing $z(t) = r(t)e^{i\psi(t)}$ and marginalising (17) over I we obtain the probability density function

$$p(\theta,t) = \frac{1-r^2(t)}{2\pi\{1-2r(t)\cos[\theta-\psi(t)]+r^2(t)\}} \tag{31}$$

which is a unimodal function of θ with maximum at $\theta = \psi$, and whose sharpness is governed by the value of r [42, 39]. For an alternative interpretation, we follow [50] and define

$$w \equiv \frac{1-\bar{z}}{1+\bar{z}} = \frac{1+2ir\sin\psi - r^2}{1+2r\cos\psi+r^2}. \tag{32}$$

In the continuum limit, the firing rate of (8), f, is equal to the flux through $\theta = \pi$, i.e.

$$f = v(I,\pi,t)p(\pi,t) = \frac{\mathrm{Re}(w)}{\pi}. \tag{33}$$

If $V = \tan(\theta/2)$ we can show using (31) that the expected value of V in the original quadratic integrate-and-fire network, $\widehat{V}$, is given by $\widehat{V} = \mathrm{Im}(w)$. Writing (30) in terms of w we obtain

$$\frac{dw}{dt} = iI_0 + \Delta - iw^2 + i(gQ+\kappa S) - gw \tag{34}$$

and writing $w = \pi f + i\widehat{V}$, (34) becomes the two real equations

$$\frac{df}{dt} = \frac{\Delta}{\pi} + 2f\widehat{V} - gf \tag{35}$$

$$\frac{d\widehat{V}}{dt} = I_0 - \pi^2 f^2 + \widehat{V}^2 + g(Q-\widehat{V}) + \kappa S \tag{36}$$

where Q and S can be determined as functions of w by writing $z = (1-\bar{w})/(1+\bar{w}) = (1-\pi f+i\widehat{V})/(1+\pi f-i\widehat{V})$. Equations (35)-(36) provide a description equivalent to (30), but we will study (30) and its analogues, and will sometime use (32)-(33) to extract the meaningful quantity f from a calculation. Note that setting $g = 0$ and $S = f$ in (35)-(36) we obtain equations (12a) and (12b) in [50]. (The replacement of S with f is a result of [50] defining synaptic dynamics slightly differently than in (10).)

The system (30) and (20) was analysed by [48] for $g = 0$ (i.e. no gap junction coupling) and $\tau = 0$ (instantaneous synapses). They found that the system supported stable fixed points, stable periodic orbits, and sometimes the coexistence of these, depending on parameter values. We will now examine two cases, focussing on the effects of $g > 0$.

2.1. **Results (excitatory coupling).** We take $\tau = 0$ for simplicity, set $\Delta = 0.05$, and consider $I_0 = -0.3$, i.e. a case where most neurons are quiescent when uncoupled. Luke et al. [48] found that for $g = 0$, there was a range of κ values for which the system had three fixed points, two of which were stable, and otherwise only one fixed point existed, and this was stable, as shown in Fig. 1.

We investigate the effect of gap junction coupling on this dynamics by numerically following fixed points and their bifurcations. The results are shown in Fig. 2, where various bifurcation curves are shown. In regions A,E and F there is one fixed point; it is stable in regions A and F, and unstable in E. In regions B,C and D there are three fixed points; only one is stable in regions B and C, and two are stable in region D. A stable periodic orbit exists in regions C and E. There is bistability only in regions C and D. We see that (for this parameter set) including gap junctions (i.e. increasing g from 0) can induce oscillations via a Hopf bifurcation, and destroy bistability.

Figure 3 shows the dynamics as g is increased from zero at $\kappa = 1.3$, i.e. passing from region D to C. In region D there is a stable fixed point, and the (constant) mean frequency f of the network is plotted in panel (a) of Fig. 3. As g is increased this fixed point undergoes a supercritical Hopf bifurcation, leading to oscillations in z, and thus in f. The maximum and minimum of f during one period of oscillation are also shown in panel (a) of Fig. 3. The period of this macroscopic oscillation is shown in panel (b) of Fig. 3; it increases rapidly as the homoclinic bifurcation is approached. This scenario is qualitatively the same as that observed by [22].

Figure 4 shows the behaviour of both a finite network (8) and the continuum description (30) and (20) at a point in region A in Fig. 2. We see that most neurons are quiescent, as reflected by the very low firing rate f. The magnitude of z is close to 1, indicating that the phases of the oscillators are very similar. The argument of z gives the

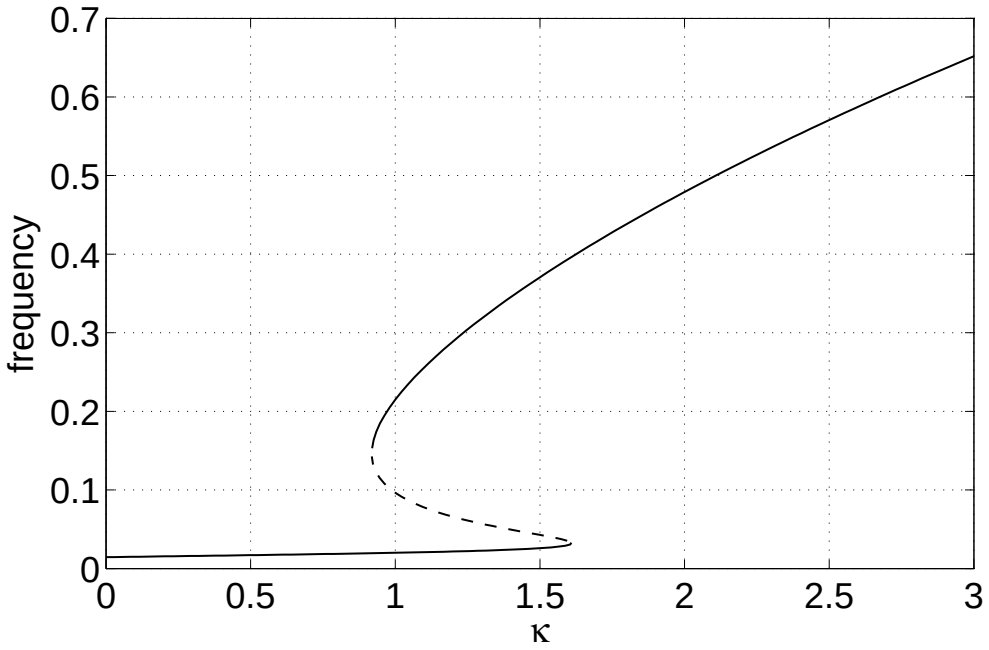

FIGURE 1. Average firing rate (from (33)) at fixed points of (30) as a function of κ for $g = 0$. Solid: stable; dashed: unstable. Parameters: $\tau = 0, I_0 = -0.3, \Delta = 0.05$.

average of the phases — it is close to -1, i.e. near the stable fixed point of an uncoupled neuron with subthreshold input.

Figure 5 shows similar behaviour but for a point in region E, clearly showing the macroscopic oscillations in both the order parameter z and the instantaneous firing rate f. Figure 6 shows the long time average firing frequency of neurons for the parameter values used in Fig. 5. We see that while several hundred of the neurons are synchronised and fire at the same frequency at which the mean field oscillates, i.e. once per oscillation, the majority are not synchronised and fire at a higher frequency.

2.2. **Results (inhibitory coupling).** We next consider the case $\kappa = -9$ (i.e. strong inhibitory synaptic coupling), keeping $\tau = 0, \Delta = 0.05$. Varying I_0 with $g = 0$ we find the scenario shown in Fig. 7. For these parameter values there is a small range of I_0 values for which the system shows bistability, either between two fixed points, or between a periodic orbit and a fixed point.

The results of increasing g are shown in Fig. 8. (The leftmost saddle-node bifurcation is not shown, as it only involves unstable solutions.) The Hopf bifurcation changes from supercritical to subcritical as g is increased, corresponding to the start of the curve of

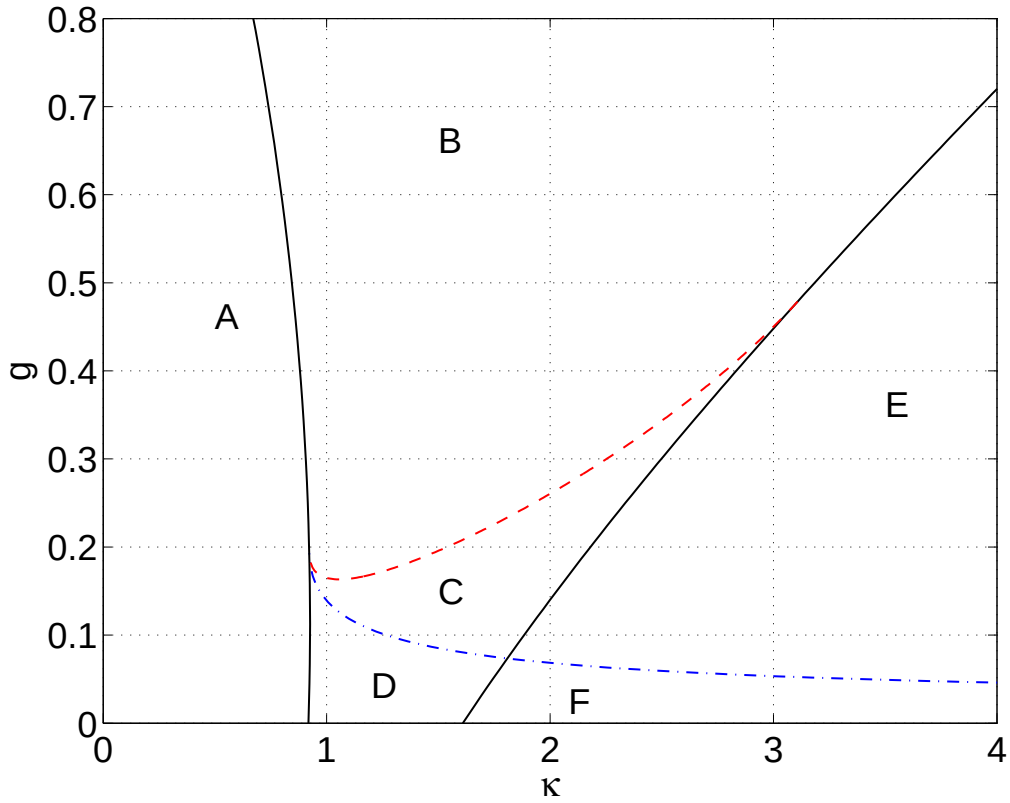

FIGURE 2. Bifurcations of (30) and (20). Solid black curves: saddle-node bifurcations of fixed points; dashed red curve: homoclinic bifurcation; dash-dotted blue curve: Hopf bifurcation. Fig. 1 corresponds to a horizontal "slice" through this Figure at $g = 0$, while Fig. 3 corresponds to a vertical "slice" at $\kappa = 1.3$. See text for further explanation. Parameters: $\tau = 0, I_0 = -0.3, \Delta = 0.05$.

saddle-node bifurcations of periodic orbits (magenta). For simplicity we only describe the dynamics in the large regions A,B,C and D. There are three fixed points in regions A,B and C, and only one (which is stable) in region D. In region A only one fixed point is stable, whereas in regions B and C two are stable, and thus there is bistability in regions B and C. We see that (roughly speaking, and for this parameter set) increasing g stabilises a fixed point with high average firing frequency (in regions B and C). The results shown in Fig. 8 have been verified in simulations of appropriate finite networks of neurons (not shown).

We now move on to study networks with spatial structure.

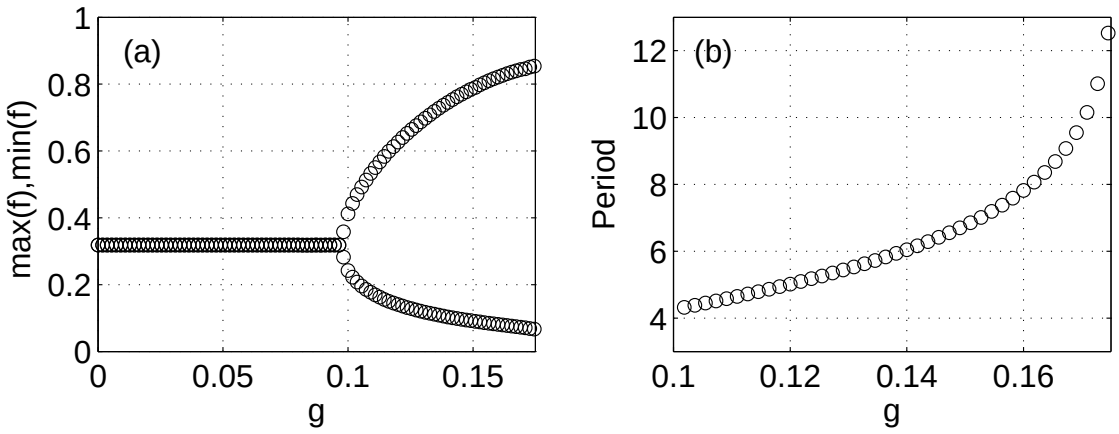

FIGURE 3. Hopf and homoclinic bifurcations in regions D and C in Fig. 2. (a): maximum and minimum of f over one oscillation. (b): period of the macroscopic oscillation. $\kappa = 1.3$. Other parameters as in Fig. 2.

3. One spatial dimension

We consider N QIF neurons, equally-spaced on a one-dimensional domain of length L, with periodic boundary conditions. Each neuron is connected via a gap junction with strength g to its M neighbours either side, a coupling previously used by [29], for example. (Since gap junctions occur when the bodies of two neurons touch, it is natural for this type of coupling to be relatively local.) Thus the dynamics without synapses are

$$\frac{dV_j}{dt} = I_j + V_j^2 + \frac{g}{2M+1}\sum_{k=j-M}^{j+M}(V_k - V_j) \tag{37}$$

for $j = 1, 2, \ldots N$, where indices are taken mod N. Changing variables and approximating the tan term as in Sec. 2 we obtain

$$\frac{d\theta_j}{dt} = 1 - \cos\theta_j - g\sin\theta_j + (1+\cos\theta_j)\left[I_j + \frac{g}{2M+1}\sum_{k=j-M}^{j+M} q(\theta_k)\right] \tag{38}$$

Including synaptic coupling we have

$$\frac{d\theta_j}{dt} = 1 - \cos\theta_j - g\sin\theta_j + (1+\cos\theta_j)\left[I_j + \frac{g}{2M+1}\sum_{k=j-M}^{j+M} q(\theta_k) + s_j\right] \tag{39}$$

where each s_j satisfies

$$\tau\frac{ds_j}{dt} = \frac{a_n L}{N}\sum_{k=1}^{N} w_{jk}(1-\cos\theta_k)^n - s_j \tag{40}$$

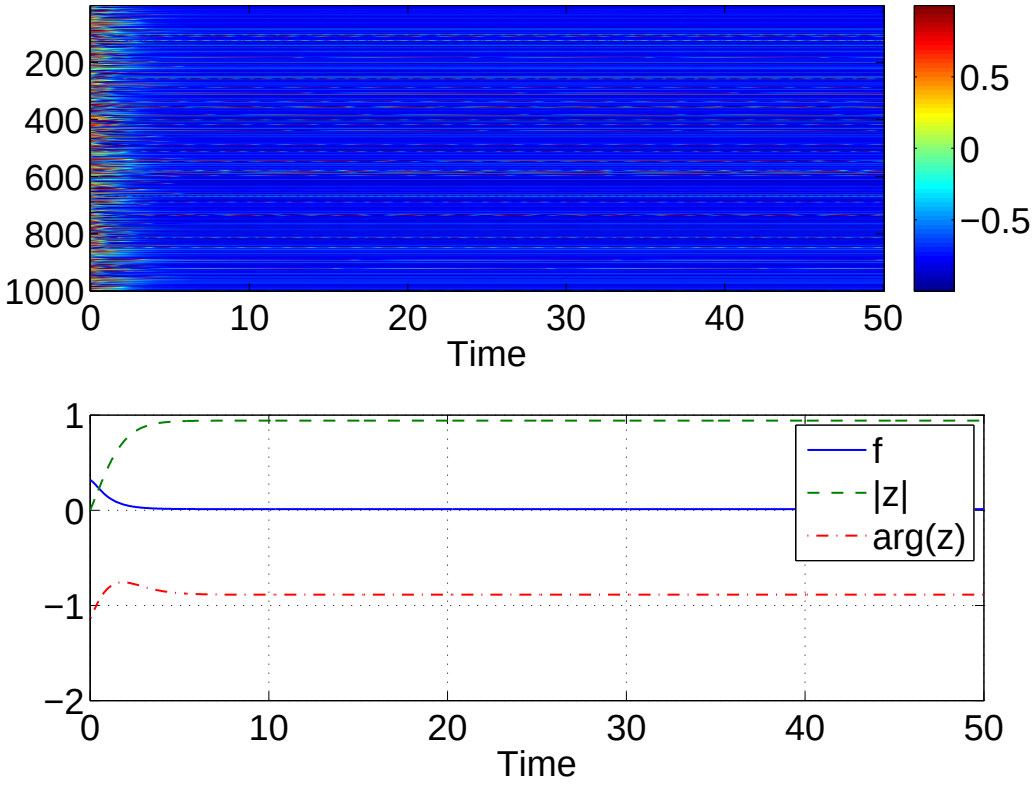

FIGURE 4. Top: $\sin\theta$ for $N = 1000$ model neurons. Bottom: results of simulating (30) and calculating f using (32)-(33). Parameters: $\kappa = 0.5, g = 0.4, \tau = 0, I_0 = -0.3, \Delta = 0.05$.

the n and a_n are as above and

$$w_{jk} = w(|j-k|\Delta x) \tag{41}$$

where $\Delta x = L/N$ and the coupling function w will be specified below. The coupling strength between neurons depends only on the distance between them; this type of coupling is commonly used in neural field modelling [13, 20, 15].

Taking the limit $N, M \to \infty$ in such a way that $M/N \to \alpha$, where $0 < \alpha < 1/2$, we describe the system by the probability density function $F(x, I, \theta, t)$. This satisfies (12), but with

$$v(x, I, \theta, t) \equiv 1 - \cos\theta - g\sin\theta + (1+\cos\theta)\left[I + gQ(x,t) + S(x,t)\right] \tag{42}$$

where

$$Q(x,t) = \int_0^L C(x-y) \int_{-\infty}^{\infty} \int_0^{2\pi} F(y, I, \theta, t) q(\theta)\, d\theta\, dI\, dy \tag{43}$$

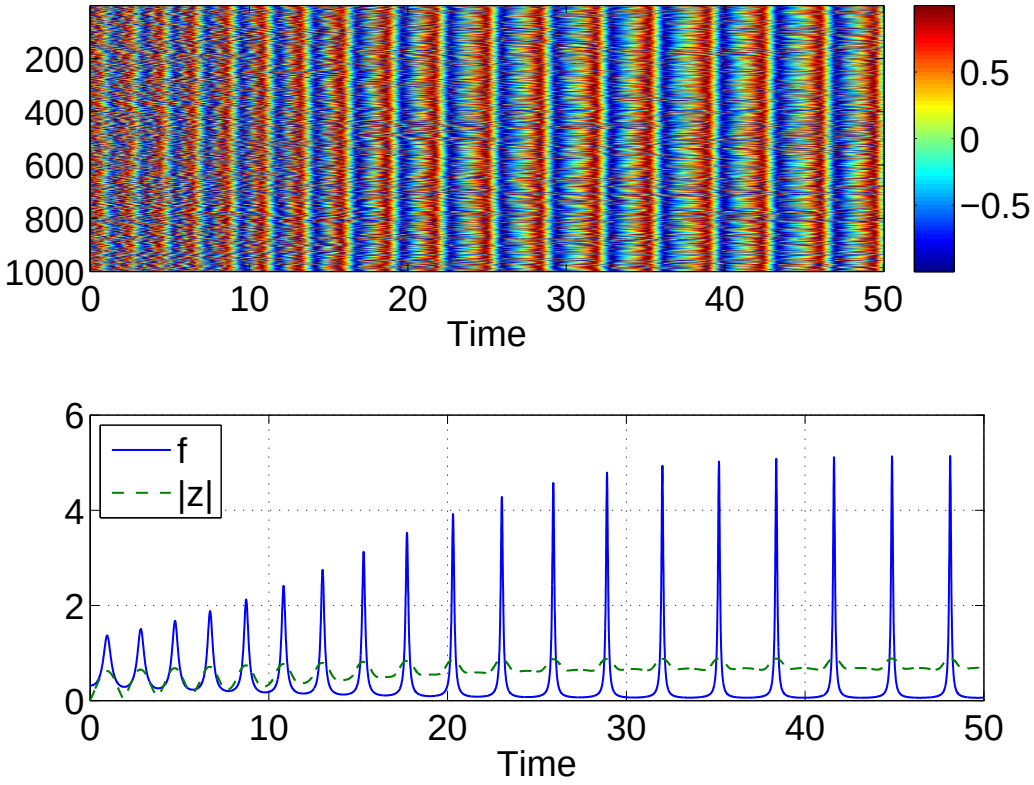

FIGURE 5. Top: $\sin\theta$ for $N = 1000$ model neurons. Bottom: results of simulating (30) and calculating f using (32)-(33). Parameters: $\kappa = 3, g = 0.2, \tau = 0, I_0 = -0.3, \Delta = 0.05$.

and

$$C(x) = \begin{cases} \frac{1}{2\alpha L}, & |x| < \alpha L \\ 0, & \text{otherwise} \end{cases} \tag{44}$$

and S satisfies

$$\tau \frac{\partial S(x,t)}{\partial t} = \int_0^L w(x-y) \int_{-\infty}^{\infty} \int_0^{2\pi} F(y,I,\theta,t) a_n (1-\cos\theta)^n \, d\theta \, dI \, dy - S(x,t) \tag{45}$$

where the spatial integrals are evaluated using periodic boundary conditions. Note that as $\alpha \to 0$, i.e. the spatial extent of the gap junction coupling tends to zero, $C(x) \to \delta(x)$ and we have

$$Q(x,t) = \int_{-\infty}^{\infty} \int_0^{2\pi} F(x,I,\theta,t) q(\theta) \, d\theta \, dI. \tag{46}$$

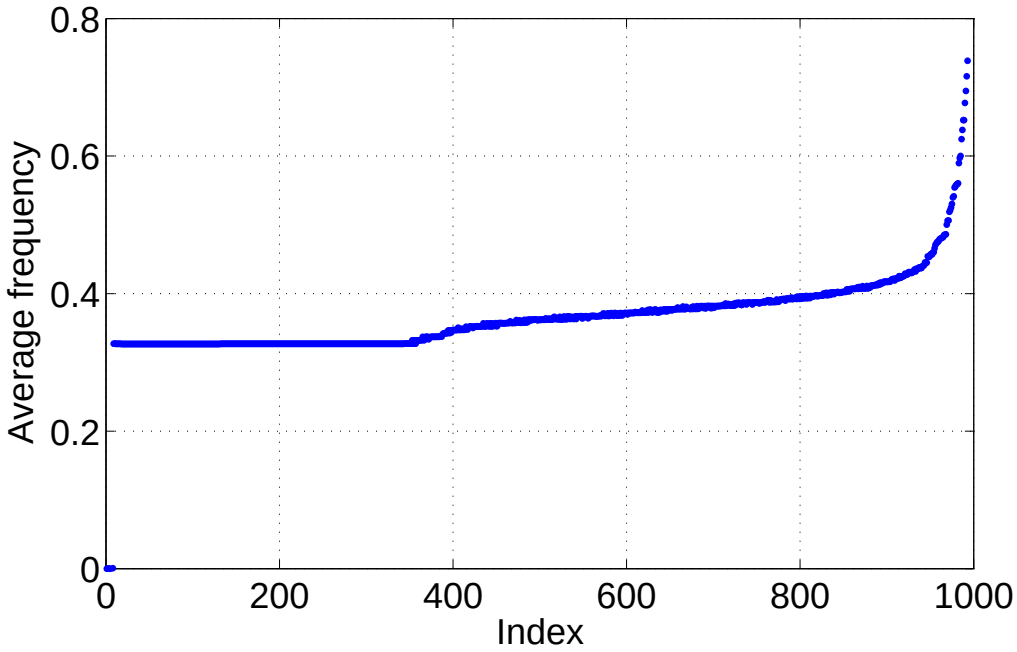

FIGURE 6. Average firing frequency of neurons for the simulation in Fig. 5. The neurons have been ordered by their I_j value, and the vertical scale has been truncated. Note that several neurons are quiescent.

Defining the spatial order parameter

$$z(x,t) \equiv \int_{-\infty}^{\infty} \int_{0}^{2\pi} F(x,I,\theta,t) e^{i\theta} \, d\theta \, dI \tag{47}$$

and repeating the analysis in Sec. 2 we obtain

$$\frac{\partial z}{\partial t} = \frac{(iI_0 - \Delta)(1+z)^2 - i(1-z)^2}{2} + \frac{i(1+z)^2(gQ+S) + g(1-z^2)}{2} \tag{48}$$

where

$$Q(x,t) = \int_0^L C(x-y) \sum_{m=1}^{\infty} \{b_m [z(y,t)]^m + \text{c.c.}\} \, dy \tag{49}$$

and $S(x,t)$ satisfies

$$\tau \frac{\partial S(x,t)}{\partial t} = \int_0^L w(x-y) H[z(y,t);n] \, dy - S(x,t) \tag{50}$$

where the b_m and the function H are as in Sec. 2. Setting $g = 0$ and $\tau = 0$ we obtain the model briefly presented in [42]. In this section we concentrate on investigating the

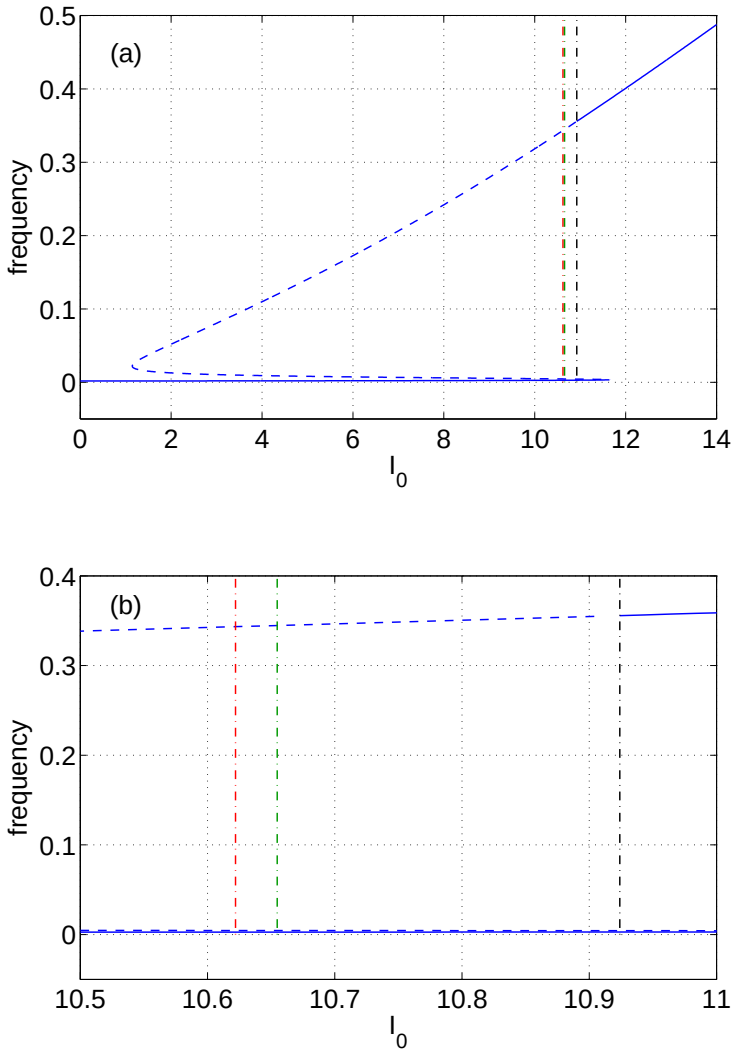

FIGURE 7. Average firing rate (from (33)) at fixed points of (30) as a function of I_0 for $g = 0$. Solid: stable; dashed: unstable. As I_0 is increased a stable and unstable periodic orbit are created in a saddle-node bifurcation (red dash-dotted line). The unstable one is destroyed in a homoclinic bifurcation (green dash-dotted line) and the stable one is destroyed in a supercritical Hopf bifurcation (black dash-dotted line). Panel (b) shows detail of (a). Parameters: $\tau = 0, \kappa = -9, \Delta = 0.05$.

effects of having $g \neq 0$. For simplicity we will set $\tau = 0$, i.e. we have

$$S(x,t) = \int_0^L w(x-y)H[z(y,t);n]\,dy \tag{51}$$

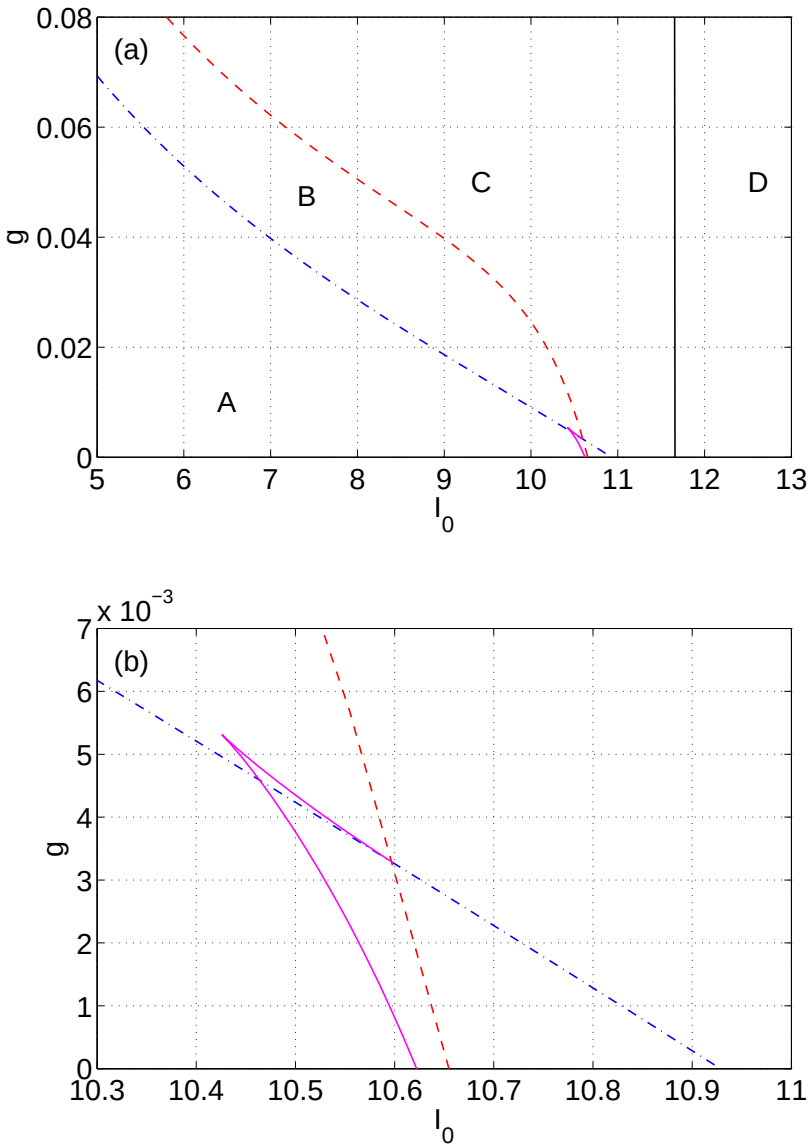

FIGURE 8. Bifurcations of (30) and (20). Solid black curve: saddle-node bifurcation of fixed points; red dashed curve: homoclinic bifurcation; blue dash-dotted curve: Hopf bifurcation; solid magenta curve: saddle-node bifurcation of periodic orbits. Fig. 7 corresponds to a horizontal "slice" through this Figure at $g = 0$. Panel (b) is an enlargement of panel (a). See text for further explanation. Parameters: $\tau = 0, \kappa = -9, \Delta = 0.05$.

The frequency profile of a solution can be calculated using the spatial version of (32)-(33), and we will use this to visualise solutions.

3.1. **Mexican hat coupling.** First consider Mexican hat coupling, as in [42]. We choose $L = 2\pi$ and $w(x) = 0.2 + 0.6\cos x$. Setting $g = 0$ we obtain the behaviour shown in Fig. 9, where the mean drive, I_0, is varied and we plot quantities related to the spatial frequency profile. The spatially uniform state shows the expected "S-shaped" curve for net positive feedback (the average of w, in this case). This state undergoes two pitchfork bifurcations, creating "one-bump" states which have spatial structure, as previously seen in [38], for example. For different values of I_0, either one, two or three different states are stable, hence the interest in such models for understanding working memory [9, 45, 65]. (The numerical results were obtained by discretising the integrals in (49) and (51) using a spatially-uniform grid of several hundred points and then following the fixed points of (48) as parameters were varied. Bifurcations were detected by determining the stability of these fixed points (from the eigenvalues of the linearisation of (48) about them) in the usual way [43, 19].)

In order to understand the effects of including gap junction coupling we will increase g from zero when $I_0 = -0.35$. From Fig. 9 we see that at this value of I_0 there exist three stable solutions (two spatially-uniform and one bump) and three unstable solutions (one spatially-uniform and two bump). The results are shown in Fig. 10. We see that as g is increased, two of the stable solutions that exist at $g = 0$ successively become unstable. (The spatially uniform solution with low average firing rate remains stable as g is increased). The first solution to become unstable is the spatially-uniform state with high average frequency. This undergoes a Hopf bifurcation at $g \approx 0.1$. It is not clear whether this bifurcation is subcritical or supercitical, but for $g = 0.2$ an initial condition near this state rapidly approaches the bump state, which is stable (results not shown). The second solution to become unstable as g is increased is the bump solution. This undergoes a Hopf bifurcation, which appears to be supercritical. Fig 11 shows the behaviour of the bump state when g is increased step-wise. The oscillations after the bifurcation are clear. One interesting observation concerns the long time average firing frequency of the solution shown in Fig. 11, as plotted in Fig. 12. Without gap junction coupling we see the typical "bump" profile, but once gap junctions are included the bump top flattens, indicating that neurons in the centre are synchronised. This does happen, as shown in Fig. 13 where we have simulated the discrete network (39) with $N = 4096$ neurons for a long time, for $g = 0$ (left) and $g = 0.6$ (right). The typical "bump" profile is seen before the bifurcation, and a region of synchrony in the centre of the bump after the bifurcation.

As g is increased further other spatiotemporal patterns may become stable. For example, the travelling wave shown in Fig. 14 is stable when $g = 1$. For this wave, the

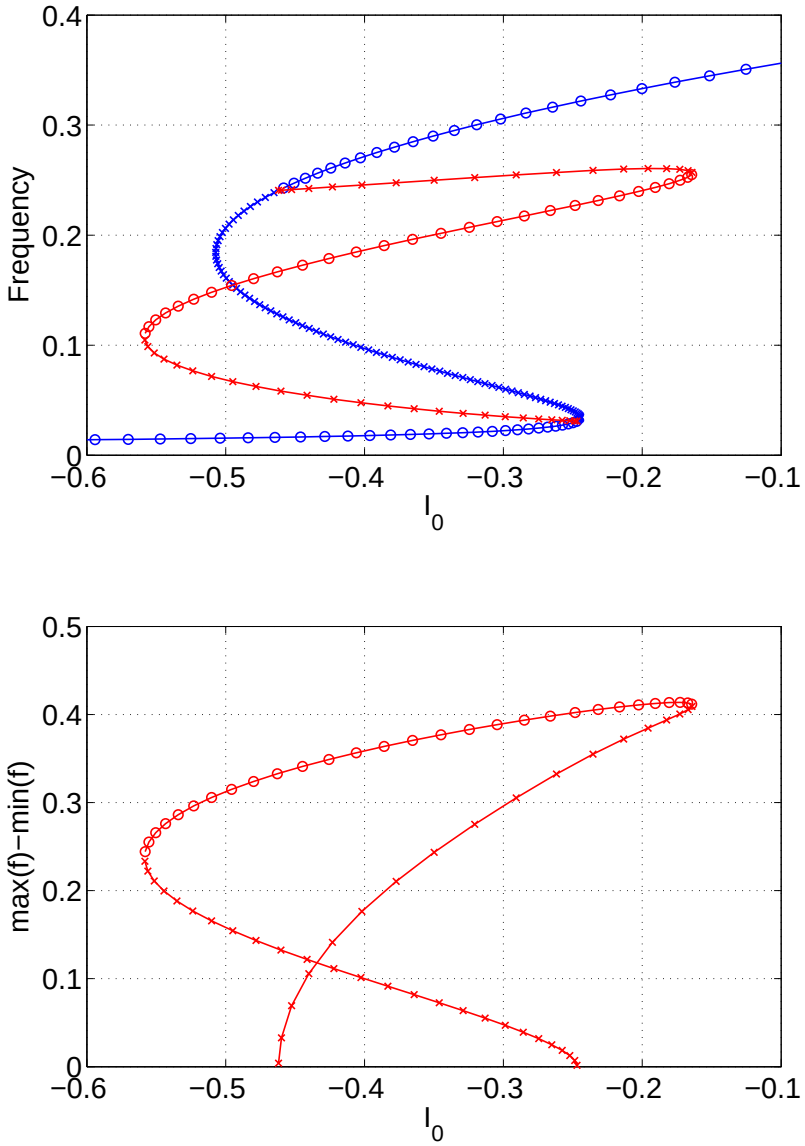

FIGURE 9. The steady states of (48), (49) and (51). Top: average firing frequency over the whole network for spatially-uniform states (blue) and bump states (red). Circles indicate stable solutions and crosses, unstable. Bottom: maximum firing frequency minus minimum firing frequency, over the spatial domain. This is zero for spatially uniform states (not shown). Parameters: $g = 0, \Delta = 0.05$.

argument of z varies through π (corresponding to firing) once as we move around the domain, i.e. it is a "one-shot" wave, where at any instant in time, neurons at one point

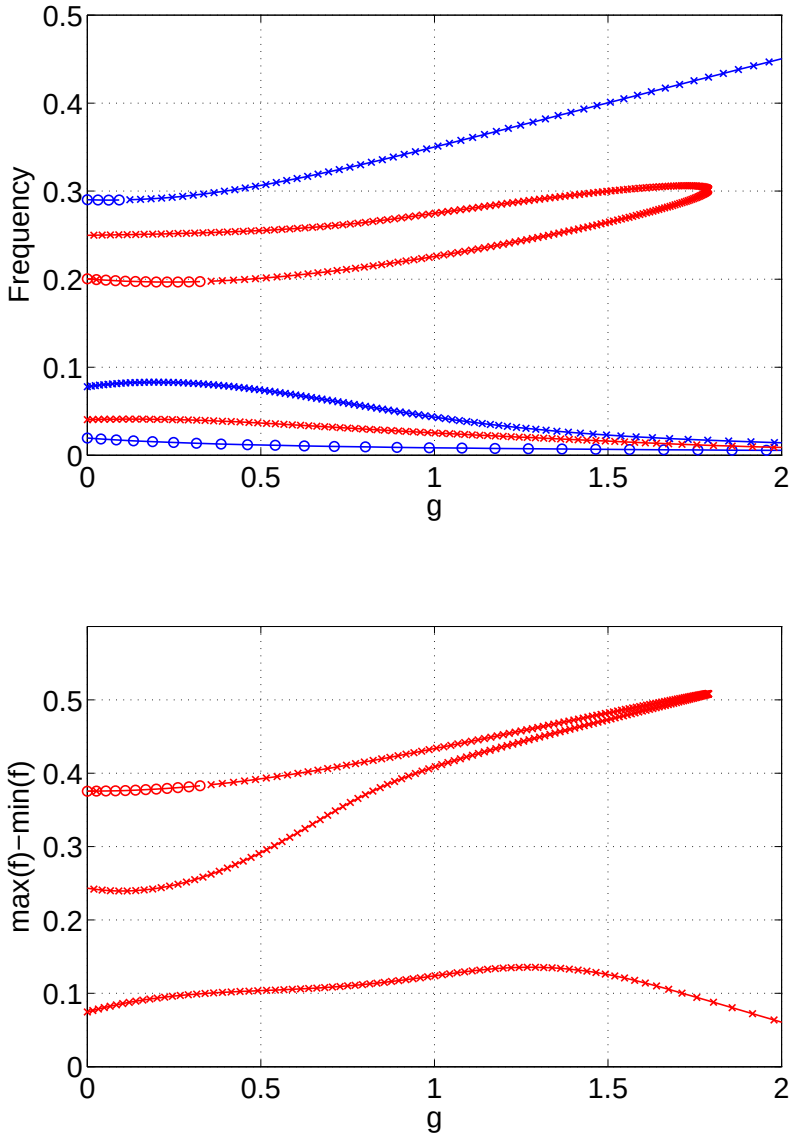

FIGURE 10. The steady states of (48), (49) and (51). Top: average firing frequency over the whole network for spatially-uniform states (blue) and bump states (red). Circles indicate stable solutions and crosses, unstable. Bottom: maximum firing frequency minus minimum firing frequency, over the spatial domain. This is zero for spatially uniform states (not shown). Parameters: $I_0 = -0.35, \Delta = 0.05, \alpha = 1/16$.

of the domain are firing, and this point travels at a constant speed around the domain. This wave is of the same form as that studied in [23], although these authors considered

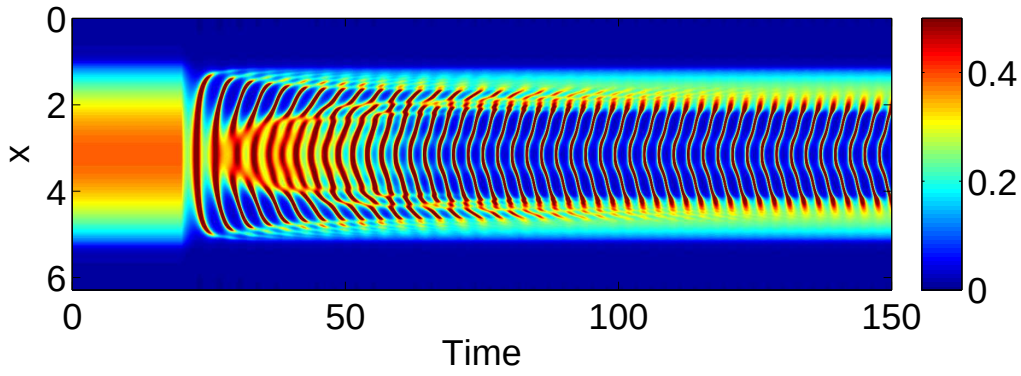

FIGURE 11. Hopf bifurcation of a bump state. f is shown colour-coded (the maximum is trucated). Gap junction coupling strength g is switched from 0 to 0.6 at $t = 20$. Parameters: $I_0 = -0.35, \Delta = 0.05, \alpha = 1/16$.

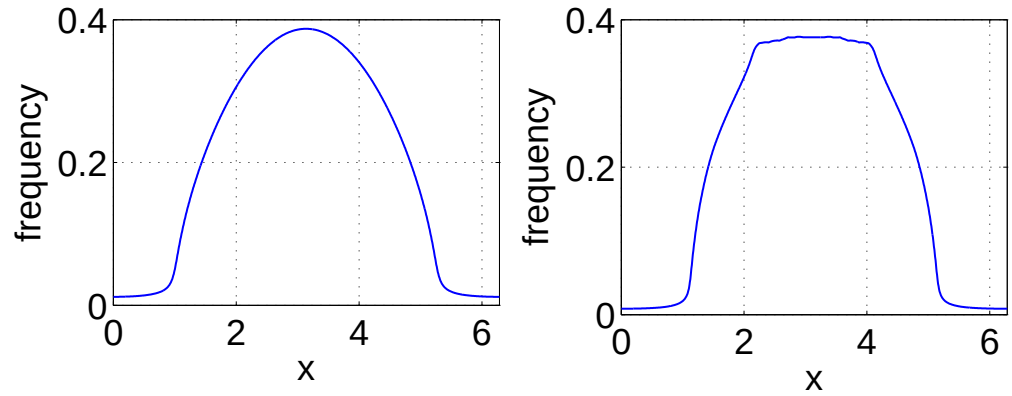

FIGURE 12. Long-time average firing frequency of the solution in Fig. 11. Left: $g = 0$, right: $g = 0.6$. Parameters: $I_0 = -0.35, \Delta = 0.05, \alpha = 1/16$.

identical neurons and no gap junction coupling. This wave travels with a constant speed and shape, and thus is stationary in a coordinate frame which is uniformly translating at the appropriate speed. Letting $\xi = x + ct$ we can write (48) as

$$\begin{aligned}\frac{\partial z(\xi,t)}{\partial t} = &-c\frac{\partial z(\xi,t)}{\partial \xi} + \frac{(iI_0-\Delta)[1+z(\xi,t)]^2 - i[1-z(\xi,t)]^2}{2} \\ &+ \frac{i[1+z(\xi,t)]^2[gQ(\xi,t)+S(\xi,t)] + g[1-z^2(\xi,t)]}{2}\end{aligned} \tag{52}$$

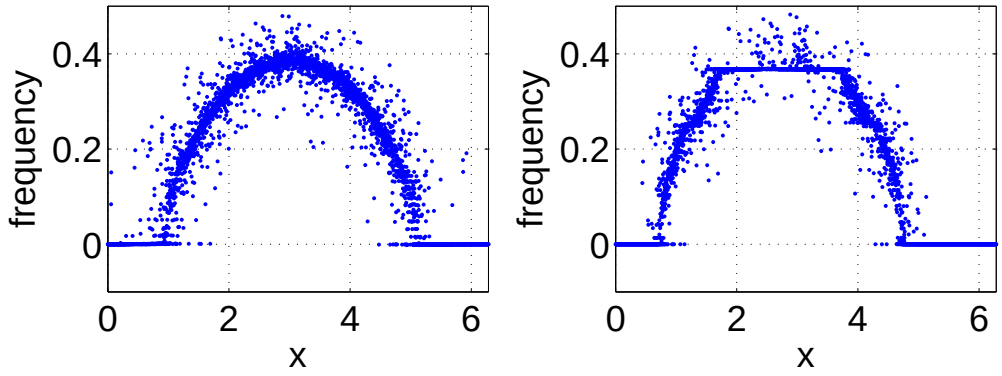

FIGURE 13. Average firing frequency for a network of $N = 4096$ neurons. Left: $g = 0$, right: $g = 0.6$. Compare with Fig. 12. Parameters: $I_0 = -0.35, \Delta = 0.05, \alpha = 1/16$.

If c is the speed of the wave shown in Fig. 14, it will be a stationary solution of (52), i.e. it will satisfy

$$0 = -c\frac{dz(\xi)}{d\xi} + \frac{(iI_0 - \Delta)[1 + z(\xi)]^2 - i[1 - z(\xi)]^2}{2} + \frac{i[1 + z(\xi)]^2[gQ(\xi) + S(\xi)] + g[1 - z^2(\xi)]}{2} \tag{53}$$

We can follow a solution of (53) as parameters are varied and determine its stability by linearising (52) about it, in the standard way [19, 43]. The results of doing this are shown in Fig. 15. As g is decreased the wave is destroyed in a saddle-node bifurcation and does not restabilise. In particular, it does not exists when $g = 0$. As g is increased it becomes unstable through a Hopf bifurcation, leading to a "breathing" wave whose shape oscillates at it travels.

While we have concentrated on the value $I_0 = -0.35$ above, the results shown are by no means all that can occur. For example, when $(I_0, g) = (0, 0.6)$, the system (48), (49) and (51) appears to show spatiotemporally chaotic solutions; see Fig. 16, top and middle panels. A simulation of the discrete network (39) shows qualitatively similar behaviour (Fig. 16, bottom panel).

The Mexican-hat connectivity function we have used with one population of neurons is an approximation to the more realistic case of two populations (excitatory and inhibitory) which have non-negative coupling functions both within and between populations [58]. Using this form of model we could then include gap junctions in either population (or with different strengths and connectivities within both populations) which is likely to be more realistic [63, 25]. The disadvantage of this is that we then have more

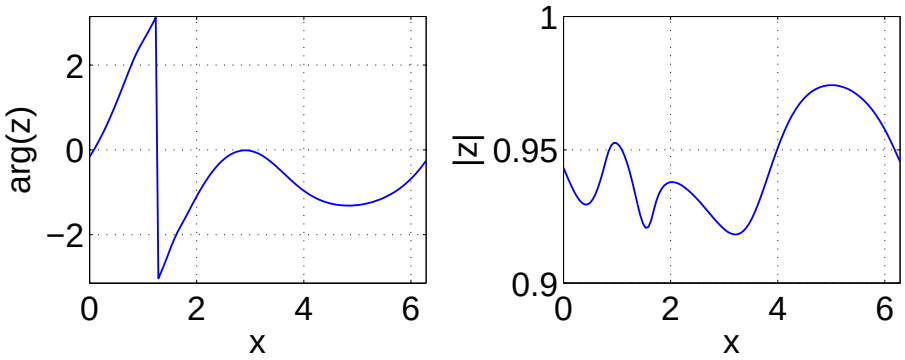

FIGURE 14. A stable travelling wave that exists for $g = 1$. It is travelling to the left. Parameters: $I_0 = -0.35, \Delta = 0.05, \alpha = 1/16$.

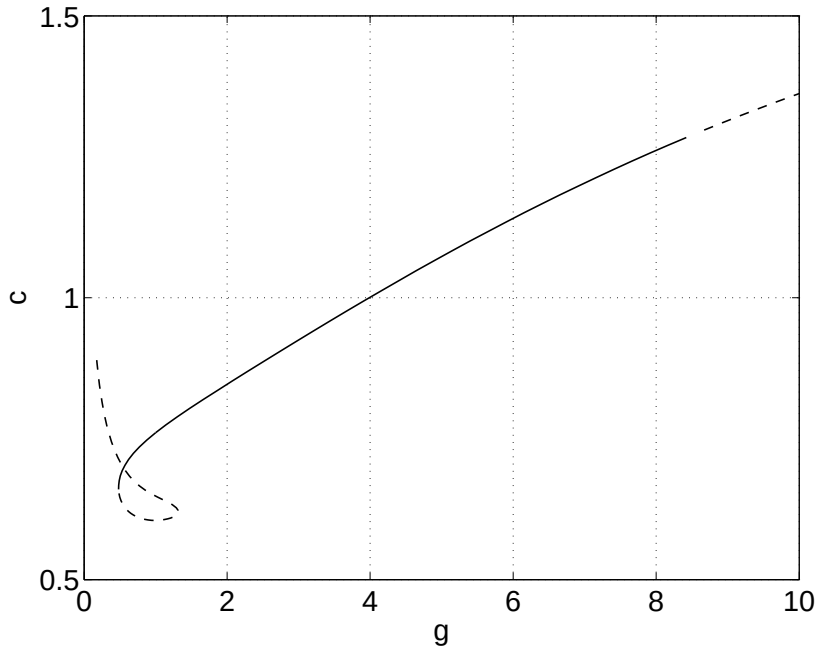

FIGURE 15. Speed of the travelling wave shown in Fig. 14. Solid curves are stable, dashed unstable. Parameters: $I_0 = -0.35, \Delta = 0.05, \alpha = 1/16$.

parameters which need to be chosen (or which could be varied), particularly if different synaptic dynamics are used for the two populations.

3.2. **Excitatory coupling.** We now consider a network with purely positive coupling, as opposed to the Mexican-hat coupling in Sec. 3.1, setting $w(x) = (3/4)e^{-|x|}$. This could model a situation in which inhibitory synaptic connections have been blocked,

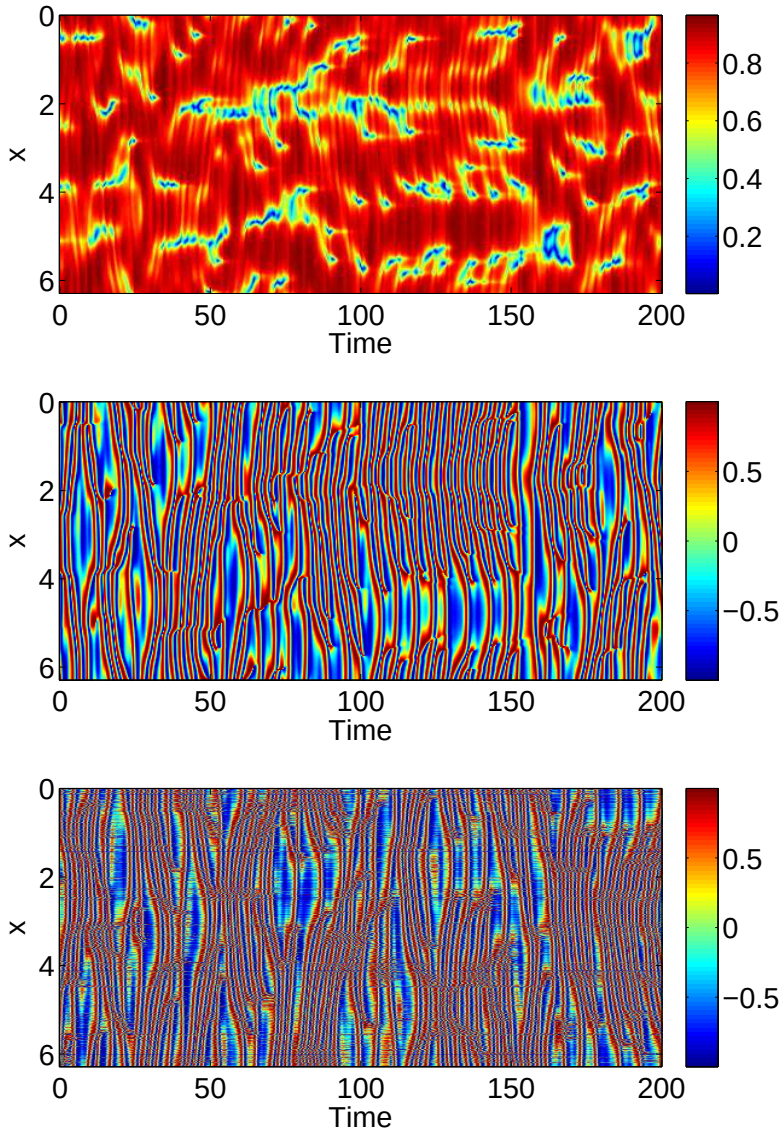

FIGURE 16. Spatiotemporal chaos. Top ($|z|$) and middle ($\sin(\arg z)$): simulation of the continuum description (48), (49) and (51). Bottom: simulation of the discrete system (39), $N = 4096$ ($\sin\theta_i$ is shown). Parameters: $g = 0.6, I_0 = 0, \Delta = 0.05, \alpha = 1/16$.

for example [57]. Because the mean of w is positive, we expect there to be a range of parameters for which two spatially uniform states are stable: one with most neurons quiescent and one with most firing incoherently. Initialising part of the domain in one of these states and the remainder in the other state, one expects to find the development

of a front connecting the two states, which will eventually move at a constant speed [40]. An example is shown in Fig. 17 on a domain of length $L = 40$ (boundary conditions are $\partial z/\partial x = 0$ at both boundaries). For these parameter values the high frequency state (left) invades the low frequency state (right). Since these waves travel with a constant speed and profile, they can be investigated in the same way as the wave shown in Fig. 14.

Starting with the wave shown in Fig. 17 and increasing g we obtain the result shown in Fig. 18. The gap junction coupling initially decreases the front speed and then destabilises it via a Hopf bifurcation. The magnitude of the corresponding eigenfunction is large where f is large and vice versa, so we expect the associated oscillations to appear in the trailing end of the wave. This is demonstrated in Fig. 19, where we instantaneously increase g once a front has developed and observe both the slowing of the front and the oscillations in its tail.

4. Two spatial dimensions

Much insight can be gained by studying a one-dimensional domain, but the layered structure of the cortex suggests that it is best treated as two-dimensional. Thus we now consider a network of neurons in a two-dimensional domain. Taking the appropriate limits the dynamics is still given by

$$\frac{\partial z}{\partial t} = \frac{(iI_0 - \Delta)(1+z)^2 - i(1-z)^2}{2} + \frac{i(1+z)^2(gQ+S) + g(1-z^2)}{2} \tag{54}$$

but we now have

$$Q(\mathbf{x},t) = \int_{\mathbb{R}^2} C(|\mathbf{x}-\mathbf{y}|)B(\mathbf{y},t)d\mathbf{y} \tag{55}$$

where

$$B(\mathbf{y},t) \equiv \sum_{m=1}^{\infty} \{b_m[z(\mathbf{y},t)]^m + \text{c.c.}\} \tag{56}$$

and (setting $\tau = 0$)

$$S(\mathbf{x},t) = \int_{\mathbb{R}^2} w(|\mathbf{x}-\mathbf{y}|)H[z(\mathbf{y},t);n]\ d\mathbf{y} \tag{57}$$

where bold indicates a two-dimensional vector. For simplicity we restrict to circularly-symmetric solutions. Moving to polar coordinates and writing $\mathbf{x} = (r,\theta)$ and $\mathbf{y} = (r',\theta')$ we have

$$Q(r,t) = \int_0^{\infty}\int_0^{2\pi} C\left(\sqrt{r^2 + r'^2 - 2rr'\cos\theta'}\right) B(r',t)r'\ d\theta'\ dr' \tag{58}$$

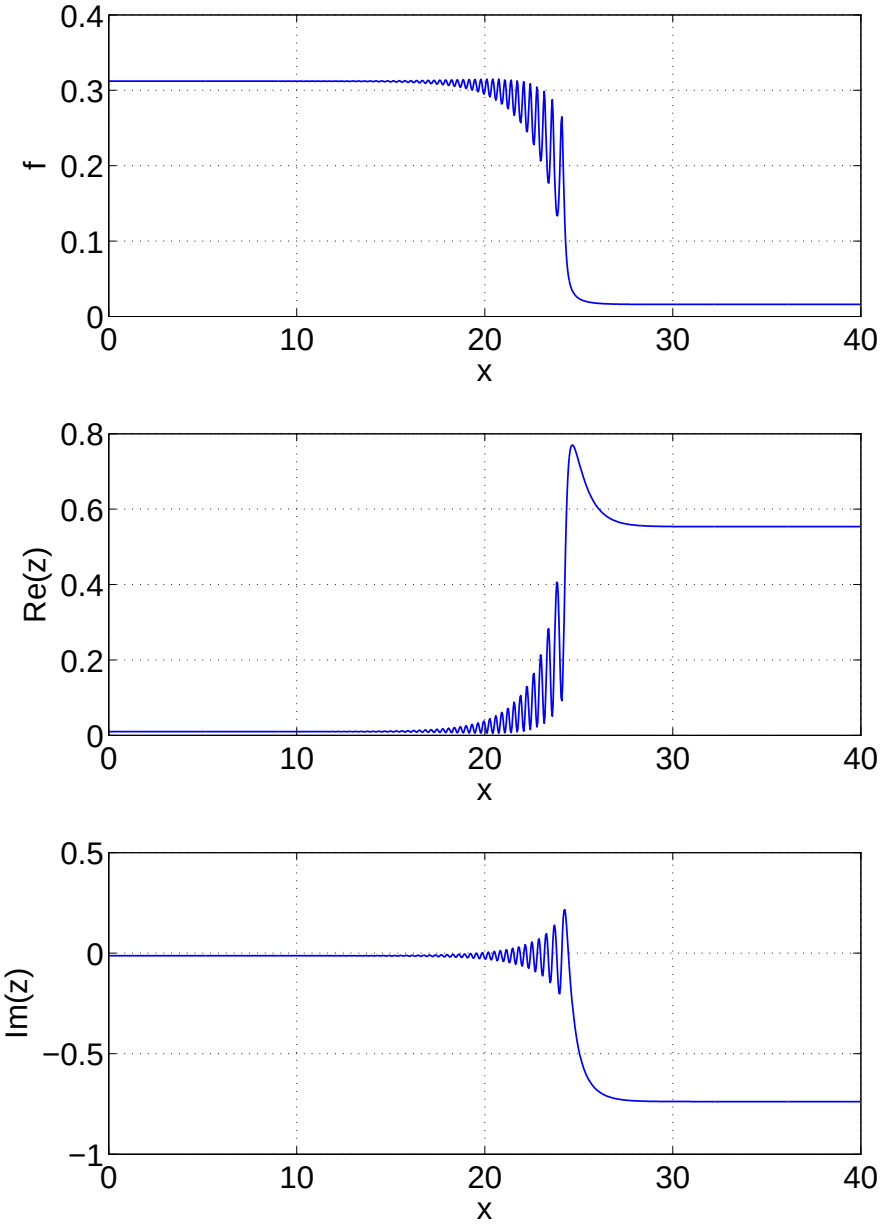

FIGURE 17. A front solution of (48), (49) and (51), travelling to the right. Top: frequency f; middle: Re(z); bottom: Im(z). Parameters: $g = 0, I_0 = -0.52, \Delta = 0.05, L = 40$.

where, without loss of generality, we have set $\theta = 0$. Defining $\tilde{C}(\rho)$ to be the Hankel transform of C, i.e.

$$\tilde{C}(\rho) = \int_0^\infty C(r) J_0(\rho r) r \, dr \tag{59}$$

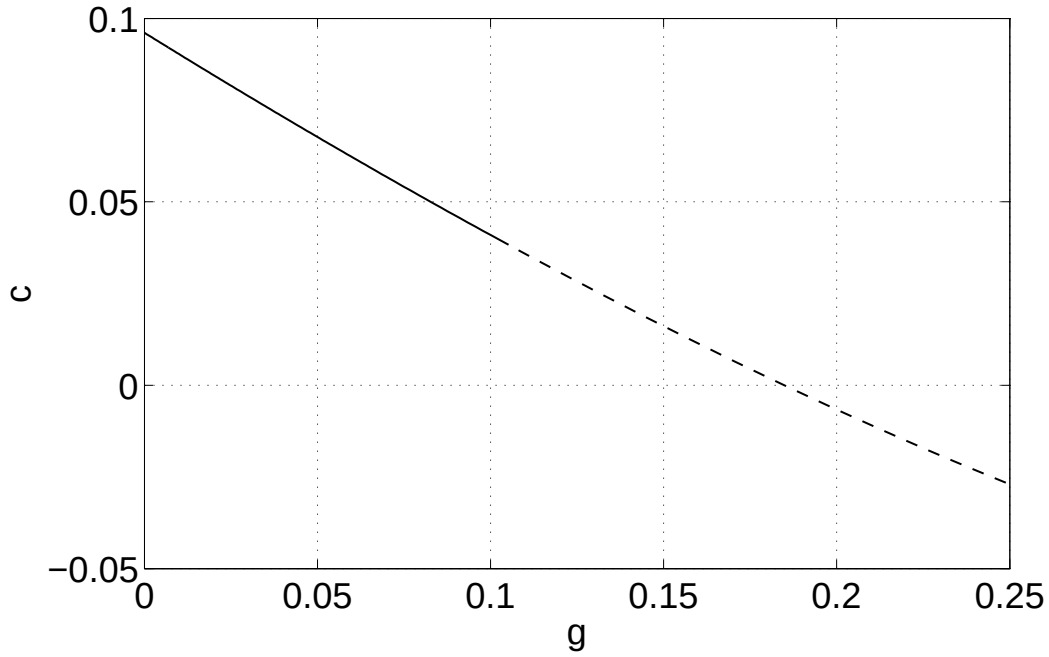

FIGURE 18. Speed of a front solution of (48), (49) and (51). Solid: stable, dashed: unstable. Neurons are jap junction coupled to those within a distance of 2.5 spatial units either side. Parameters: $I_0 = -0.52, \Delta = 0.05, L = 40$.

where J_0 is the Bessel function of the first kind of order 0, we have

$$C(r) = \int_0^\infty \tilde{C}(\rho) J_0(\rho r) \rho \, d\rho \tag{60}$$

and substituting into (58) we have

$$Q(r,t) = \int_0^\infty \int_0^{2\pi} \int_0^\infty \tilde{C}(\rho) J_0\left(\rho\sqrt{r^2 + r'^2 - 2rr'\cos\theta'}\right) B(r',t) \rho r' \, d\rho \, d\theta' \, dr' \tag{61}$$

Using a summation theorem for Bessel functions [8, 27] and integrating over θ' we find

$$\begin{aligned} Q(r,t) &= 2\pi \int_0^\infty \int_0^\infty \tilde{C}(\rho) J_0(\rho r) J_0(\rho r') B(r',t) \rho r' \, d\rho \, dr' \\ &= 2\pi \int_0^\infty B(r',t) r' \int_0^\infty \tilde{C}(\rho) J_0(\rho r) J_0(\rho r') \rho \, d\rho \, dr' \end{aligned} \tag{62}$$

If, for example,

$$C(r) = \frac{e^{-r^2/(2\alpha^2)}}{2\pi\alpha^2} \tag{63}$$

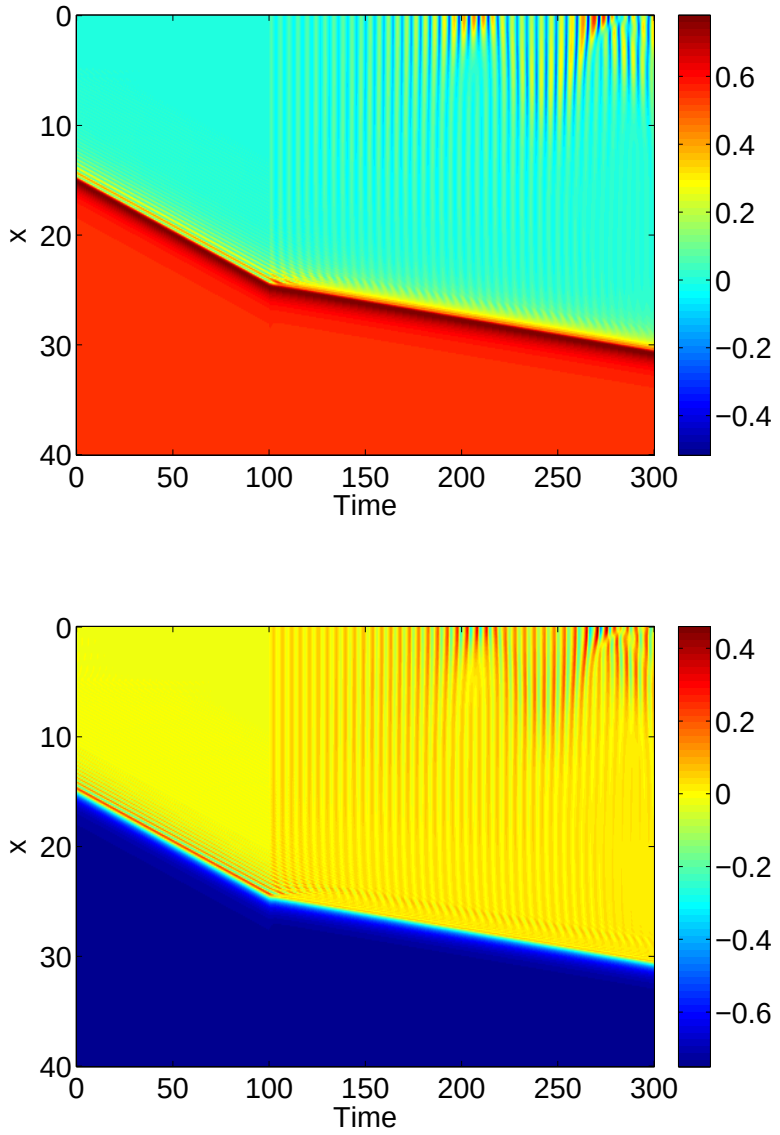

FIGURE 19. Top: Re(z). Bottom: Im(z). g is switched from 0 to 0.12 at $t = 100$. Neurons are jap junction coupled to those within a distance of 2.5 spatial units either side. Parameters: $I_0 = -0.52, \Delta = 0.05, L = 40$.

i.e. neurons are gap junction coupled with a strength which is Gaussian in distance, with characteristic length α, then

$$\tilde{C}(\rho) = \frac{e^{-\alpha^2\rho^2/2}}{2\pi} \tag{64}$$

and

$$\int_0^\infty \tilde{C}(\rho)J_0(\rho r)J_0(\rho r')\rho\ d\rho = \frac{1}{2\pi\alpha^2}I_0\left(\frac{rr'}{\alpha^2}\right)\exp\left(\frac{-(r^2+r'^2)}{2\alpha^2}\right) \tag{65}$$

where I_0 is the modified Bessel function of the first kind of order 0 and thus

$$Q(r,t) = \frac{1}{\alpha^2}\int_0^\infty B(r',t)I_0\left(\frac{rr'}{\alpha^2}\right)\exp\left(\frac{-(r^2+r'^2)}{2\alpha^2}\right)r'\ dr' \tag{66}$$

Note that

$$\int_0^{2\pi}\int_0^\infty C(r)rdrd\theta = 1 \tag{67}$$

independent of α. Now (57) is of the same form as (55), i.e. a two-dimensional convolution, so we can write

$$S(r,t) = 2\pi\int_0^\infty H(r',t)r'\int_0^\infty \tilde{w}(\rho)J_0(\rho r)J_0(\rho r')\rho\ d\rho\ dr' \tag{68}$$

where we have dropped the dependence of H on n and $\tilde{w}(\rho)$ is the Hankel transform of $w(r)$. As several others have done [16, 10] we choose $w(r)$ to be a linear combination of modified Bessel functions of the second kind giving a Mexican-hat shape (see Fig. 20):

$$w(r) = 1.25K_0(r) - K_0(2r) - 0.25K_0(r/2) \tag{69}$$

We have

$$\tilde{w}(\rho) = \frac{1.25}{1+\rho^2} - \frac{1}{4+\rho^2} - \frac{0.25}{1/4+\rho^2} \tag{70}$$

and thus

$$\int_0^\infty \tilde{w}(\rho)J_0(\rho r)J_0(\rho r')\rho\ d\rho \equiv L(r,r') \tag{71}$$

$$= \begin{cases} 1.25I_0(r)K_0(r') - I_0(2r)K_0(2r') - 0.25I_0(r/2)K_0(r'/2) & \text{if } r < r' \\ 1.25I_0(r')K_0(r) - I_0(2r')K_0(2r) - 0.25I_0(r'/2)K_0(r/2) & \text{if } r' < r \end{cases}$$

and so

$$S(r,t) = 2\pi\int_0^\infty H(r',t)L(r,r')r'\ dr' \tag{72}$$

For some parameters a spatially-localised bump solution centred at the origin is stable. Following this solution as g is increased we obtain the results in Fig. 21: the stable bump solution is destroyed in a saddle-node bifurcation. (Note that the mostly quiescent state is also stable for these parameter values.)

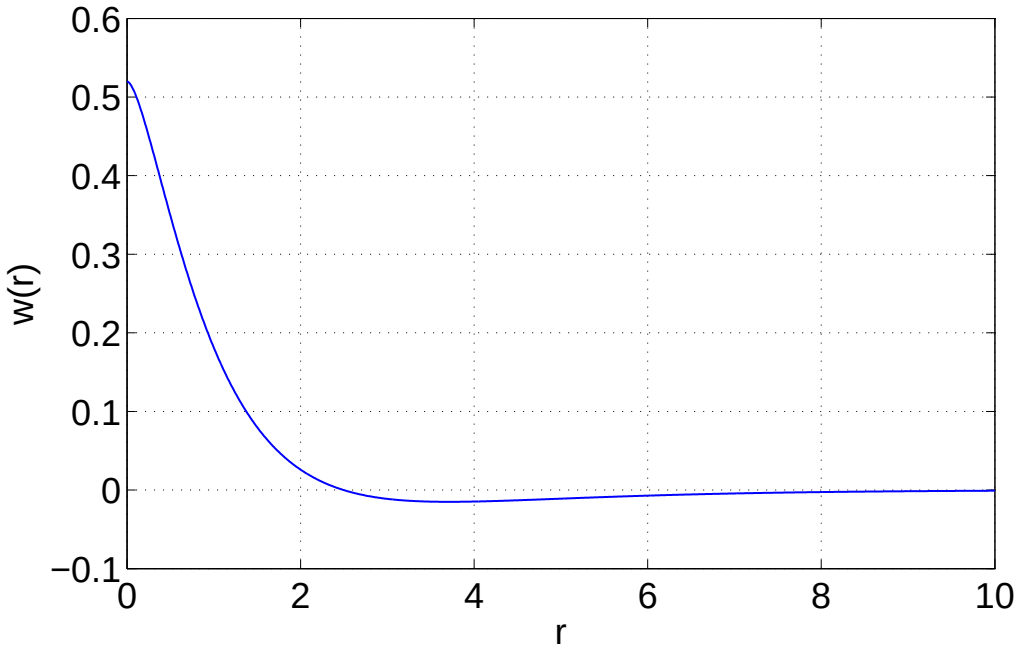

FIGURE 20. The synaptic coupling function $w(r)$ as given by (69).

Using other coupling functions such as a decaying oscillatory one may mean that the system can support more interesting solutions such as rings or multiple bump solutions [36, 59]. The stability of circularly symmetric solutions with respect to perturbations which break the circular symmetry of the underlying solution could then be investigated, as others have done for classical neural field models [10, 16, 9, 55]. Such a system may also support spiral waves [35]. Note that [52] observed both spiral and "lurching" waves in two-dimensional networks of synaptically coupled theta neurons, although they included spike frequency adaptation [5], which we have not addressed here.

5. Summary and Discussion

In conclusion, we have derived exact evolution equations describing the asymptotic dynamics of infinite networks of quadratic integrate-and-fire neurons, coupled by synapses and gap junctions, in zero, one and two spatial dimensions. In one and two spatial dimensions these equations have the form of neural field models [9, 13, 20], being nonlocal evolution equations for a macroscopic quantity, in this case a complex order parameter. Physically meaningful variables can be derived from this complex variable using the transformation (32) and then taking real and imaginary parts. We can summarise our

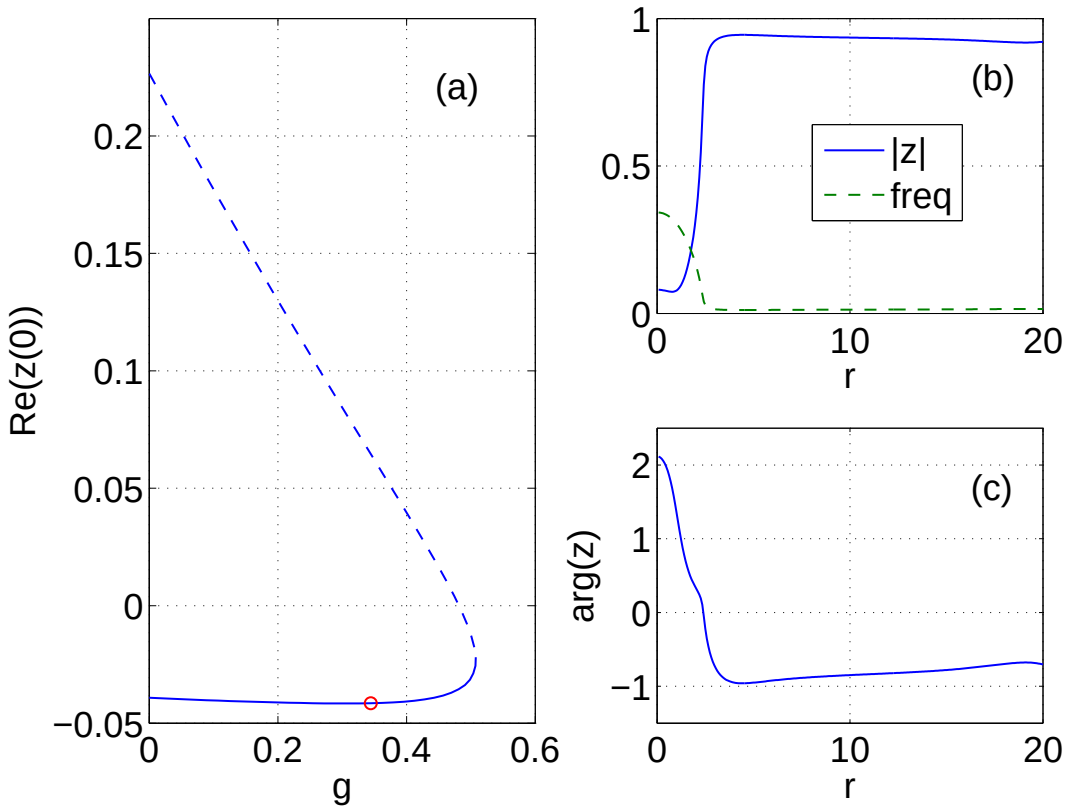

FIGURE 21. (a): Re(z) at $r = 0$ for a family of stationary solutions of (54), (66) and (72), as a function of gap junction coupling strength g. Solid: stable; dashed: unstable. (b) and (c) show the magnitude and argument of $z(r)$, and the average frequency, at the point shown by the red circle in panel (a). Parameters: $I_0 = -0.2, \Delta = 0.05, \alpha = 1$.

results by saying that (for the parameter sets we have chosen) including gap junctions removes multistability by destroying (in saddle-node bifurcations) or making unstable (through Hopf bifurcations) solutions for which the majority of neurons are firing, when synaptic connections are largely (or completely) positive. When inhibitory synaptic connections are present (as in Sec. 2.2) gap junctions act to stabilise an otherwise unstable state with high firing rate. The presence of gap junctions has little effect on solutions for which most neurons are quiescent, as it seems to only act to make the neurons' states more similar.

We now compare our results with those of others. Ermentrout [22] considered a network similar to (8) but with dynamic synapses (i.e. $\tau \neq 0$), $n = 5$, and with white noise added to the original voltage dynamics. He numerically analysed the resulting

Fokker-Planck equation and found a scenario equivalent to passing from region D to C to B in Fig. 2 as gap junction strength was increased, for both the high activity state and the low activity state, which is consistent with our results (see Fig. 3). By not including noise in our model we have been able to describe the network with a single ODE rather than a probability density function, and thus easily determine which bifurcations occur. Laing [38] considered a model similar to (39)-(40) although using leaky integrate-and-fire neurons with added white noise. Using the "equation-free" approach he followed saddle-node bifurcations of the type seen in Fig. 9 as gap junction strength was increased. That analysis relied on the synapses being sufficiently slow, so that a separation of timescales occurred, and we have not attempted a similar calculation here. Steyn-Ross et al. [63] took an established neural field model in which some of the dynamic variables are "mean voltage" and included the effects of gap junctions via diffusion acting on these mean voltages. While gap junctional coupling between spiking neurons does provide a diffusive coupling in voltage, it is not clear that their approach was correct, given that action potentials were already removed in the derivation of their original model, which describes the dynamics of population-averaged voltages and firing rates. Nevertheless, they found that including gap junctions promoted the formation of stationary Turing patterns, which is consistent with Fig. 10, where we see the spatially uniform state with high activity become unstable to a bump state as g is increased.

Clearly we have not given a complete description of the dynamics of the networks considered, and now briefly discuss various parameters that could be varied. Increasing n from $n = 2$ will sharpen the synaptic input. Setting $\tau \neq 0$ will introduce synaptic dynamics, thus increasing the number of dynamic variables. Synaptic timescales are known to be important when determining the stability of solutions, [7, 45, 58] so varying τ may introduce new dynamics. We have only considered the level of heterogeneity $\Delta = 0.05$. It is not clear whether this should be regarded as small or large, but it has been shown that increasing such a form of heterogeneity can create new types of dynamics in a model of coupled phase oscillators [41]. Concerns have also been raised by others regarding the use of the Lorentzian distribution for the heterogeneous parameter [34], and it would be interesting to investigate other distributions. As mentioned in Sec. 3.1, it would be interesting to consider two coupled populations, possibly with gap junction coupling only between inhibitory neurons; doing so would increase the number of dynamic variables. Finally, we have not considered varying the form of the coupling functions (or for the most part, their strength), either synaptic or gap junctional, or considered the possibility of only gap junctional coupling.

Note that we could use the analysis shown here to study a network in which we modelled synaptic input as conductance changes rather than current inputs. Consider, for example,

$$\frac{dV_j}{dt} = I_j + V_j^2 - s(t)(V_j - V_r) + \frac{g}{N}\sum_{k=1}^{N}(V_k - V_j) \tag{73}$$

where V_r is a reversal potential and $s(t)$ is a known function. Letting $U_j = V_j - s/2$ we have

$$\frac{dU_j}{dt} = U_j^2 + I_j + sV_r - s^2/4 - gU_j + \frac{g}{N}\sum_{k=1}^{N} U_k - \frac{1}{2}\frac{ds}{dt} \tag{74}$$

We would then proceed by letting $U_j = \tan(\theta_j/2)$.

We conclude with several more points. While we have concentrated on the case of nonidentical neurons, some progress can be made when all neurons are identical, i.e. $\Delta = 0$ and thus $I_j = I_0\ \forall j$. For the travelling wave in Sec. 3.1, in the continuum limit, we have

$$\frac{\partial\theta(x,t)}{\partial t} = 1 - \cos\theta(x,t) - g\sin\theta(x,t) + (1+\cos\theta(x,t))\left[I_0 + gQ(x,t) + S(x,t)\right] \tag{75}$$

where

$$Q(x,t) = \int_0^L C(x-y)q(\theta(y,t))\,dy \tag{76}$$

and S satisfies

$$S(x,t) = \int_0^L w(x-y)a_n(1-\cos\theta(y,t))^n\,dy \tag{77}$$

i.e. we have a description in terms of phase only. If c is the speed of the wave, the wave profile will satisfy the (nonlocal) ordinary differential equation

$$c\frac{d\theta}{d\xi} = 1 - \cos\theta - g\sin\theta + (1+\cos\theta)\left[I_0 + gQ + S\right] \tag{78}$$

where θ, Q and S are functions of $\xi = x + ct$ only. The travelling wave will be a periodic solution (with period L) of this equation.

We have only considered point neurons, with no spatial extent. However, gap junction coupling is often between cell dendrites rather than somas, so it would be of interest to extend the results presented here to spatially-extended neurons using, for example, ideas in [17]. It would also be interesting to include slow intrinsic currents to model spike frequency adaptation [5] or synaptic depression [31]. We have only considered a deterministic network of neurons, whereas noise is ubiquitous in neural systems [37]

and, for example, Ermentrout studied a network similar to that in Sec. 2 but with white noise applied to the voltage dynamics [22]. The inclusion of noise adds a diffusive term to the continuity equation (12), and the Ott/Antonsen ansatz can no longer be used to simplify the resulting Fokker-Planck equation. It can however be solved numerically, as Ermentrout did (see also [41]) and thus the effect of noise on the spatially extended networks studied here could be investigated, although this would be computationally challenging.

Acknowledgements: I thank the referees for their useful comments.

References

[1] D.M. Abrams, R. Mirollo, S.H. Strogatz, and D.A. Wiley. Solvable model for chimera states of coupled oscillators. *Phys. Rev. Lett.*, 101(8):084103, 2008.

[2] Shun-ichi Amari. Dynamics of pattern formation in lateral-inhibition type neural fields. *Biological cybernetics*, 27(2):77–87, 1977.

[3] Tiaza Bem and John Rinzel. Short duty cycle destabilizes a half-center oscillator, but gap junctions can restabilize the anti-phase pattern. *Journal of Neurophysiology*, 91(2):693–703, 2004.

[4] R Ben-Yishai, R Lev Bar-Or, and H Sompolinsky. Theory of orientation tuning in visual cortex. *Proceedings of the National Academy of Sciences, USA*, 92(9):3844–3848, 1995.

[5] Jan Benda and Andreas VM Herz. A universal model for spike-frequency adaptation. *Neural computation*, 15(11):2523–2564, 2003.

[6] Michael V.L Bennett and R. Suzanne Zukin. Electrical coupling and neuronal synchronization in the mammalian brain. *Neuron*, 41(4):495 – 511, 2004.

[7] Patrick Blomquist, John Wyller, and Gaute T Einevoll. Localized activity patterns in two-population neuronal networks. *Physica D: Nonlinear Phenomena*, 206(3):180–212, 2005.

[8] Paul C Bressloff. Spontaneous symmetry breaking in self–organizing neural fields. *Biological Cybernetics*, 93(4):256–274, 2005.

[9] Paul C Bressloff. Spatiotemporal dynamics of continuum neural fields. *Journal of Physics A: Mathematical and Theoretical*, 45(3):033001, 2012.

[10] Paul C Bressloff and Zachary P Kilpatrick. Two-dimensional bumps in piecewise smooth neural fields with synaptic depression. *SIAM Journal on Applied Mathematics*, 71(2):379–408, 2011.

[11] Paul C Bressloff and Matthew A Webber. Neural field model of binocular rivalry waves. *Journal of computational neuroscience*, 32(2):233–252, 2012.

[12] C.C. Chow and N. Kopell. Dynamics of spiking neurons with electrical coupling. *Neural Comput.*, 12(7):1643–1678, 2000.

[13] S. Coombes. Waves, bumps, and patterns in neural field theories. *Biol. Cybern.*, 93(2):91–108, 2005.

[14] Stephen Coombes. Neuronal networks with gap junctions: A study of piecewise linear planar neuron models. *SIAM Journal on Applied Dynamical Systems*, 7(3):1101–1129, 2008.

[15] Stephen Coombes, Peter beim Graben, Roland Potthast, and James Wright, editors. *Neural Fields: Theory and Applications*. Springer, 2014.

[16] Stephen Coombes, Helmut Schmidt, and Ingo Bojak. Interface dynamics in planar neural field models. *The Journal of Mathematical Neuroscience (JMN)*, 2(1):1–27, 2012.

[17] Stephen Coombes, Yulia Timofeeva, C-M Svensson, Gabriel J Lord, Krešimir Josić, Steven J Cox, and Costa M Colbert. Branching dendrites with resonant membrane: a sum-over-trips approach. *Biological Cybernetics*, 97(2):137–149, 2007.

[18] Stephen Coombes and Margarita Zachariou. Gap junctions and emergent rhythms. In *Coherent Behavior in Neuronal Networks*, pages 77–94. Springer, 2009.

[19] Eusebius Doedel, Herbert B Keller, and Jean Pierre Kernevez. Numerical analysis and control of bifurcation problems (i): Bifurcation in finite dimensions. *International journal of bifurcation and chaos*, 1(03):493–520, 1991.

[20] B. Ermentrout. Neural networks as spatio-temporal pattern-forming systems. *Rep. Prog. Phys.*, 61:353–430, 1998.

[21] Bard Ermentrout. Type I membranes, phase resetting curves, and synchrony. *Neural computation*, 8(5):979–1001, 1996.

[22] Bard Ermentrout. Gap junctions destroy persistent states in excitatory networks. *Physical Review E*, 74(3):031918, 2006.

[23] Bard Ermentrout, Jonathan Rubin, and Remus Osan. Regular traveling waves in a one-dimensional network of theta neurons. *SIAM Journal on Applied Mathematics*, 62(4):1197–1221, 2002.

[24] G. B. Ermentrout and N. Kopell. Parabolic bursting in an excitable system coupled with a slow oscillation. *SIAM Journal on Applied Mathematics*, 46(2):233–253, 1986.

[25] Takaichi Fukuda, Toshio Kosaka, Wolf Singer, and Ralf A. W. Galuske. Gap junctions among dendrites of cortical gabaergic neurons establish a dense and widespread intercolumnar network. *The Journal of Neuroscience*, 26(13):3434–3443, 2006.

[26] Jay R Gibson, Michael Beierlein, and Barry W Connors. Two networks of electrically coupled inhibitory neurons in neocortex. *Nature*, 402(6757):75–79, 1999.

[27] Izrael Solomonovich Gradshtejn and Iosif Moiseevich Ryzhik. *Table of integrals, series and products*. Academic Press, 1965.

[28] D Hansel and G Mato. Existence and stability of persistent states in large neuronal networks. *Physical Review Letters*, 86(18):4175, 2001.

[29] Fatma Gurel Kazanci and Bard Ermentrout. Pattern formation in an array of oscillators with electrical and chemical coupling. *SIAM Journal on Applied Mathematics*, 67(2):pp. 512–529, 2007.

[30] TB Kepler, E Marder, and LF Abbott. The effect of electrical coupling on the frequency of model neuronal oscillators. *Science*, 248(4951):83–85, 1990.

[31] Zachary P Kilpatrick and Paul C Bressloff. Spatially structured oscillations in a two-dimensional excitatory neuronal network with synaptic depression. *Journal of computational neuroscience*, 28(2):193–209, 2010.

[32] Nancy Kopell and Bard Ermentrout. Chemical and electrical synapses perform complementary roles in the synchronization of interneuronal networks. *Proceedings of the National Academy of Sciences of the United States of America*, 101(43):15482–15487, 2004.

[33] Y. Kuramoto. *Chemical Oscillations, Waves, and Turbulence*. Springer, Berlin, 1984.

[34] Luis F. Lafuerza, Pere Colet, and Raul Toral. Nonuniversal results induced by diversity distribution in coupled excitable systems. *Phys. Rev. Lett.*, 105:084101, Aug 2010.

[35] C. R. Laing. Spiral waves in nonlocal equations. *SIAM Journal on Applied Dynamical Systems*, 4(3):588–606, 2005.

[36] C. R. Laing and W.C. Troy. PDE methods for nonlocal models. *SIAM Journal on Applied Dynamical Systems*, 2(3):487–516, 2003.

[37] Carlo Laing and Gabriel J Lord, editors. *Stochastic methods in neuroscience*. Oxford University Press, 2009.

[38] Carlo R Laing. On the application of "equation-free modelling" to neural systems. *Journal of Computational Neuroscience*, 20(1):5–23, 2006.

[39] Carlo R. Laing. The dynamics of chimera states in heterogeneous Kuramoto networks. *Physica D*, 238(16):1569–1588, 2009.

[40] Carlo R. Laing. Fronts and bumps in spatially extended kuramoto networks. *Physica D*, 240(24):1960 – 1971, 2011.

[41] Carlo R Laing. Disorder-induced dynamics in a pair of coupled heterogeneous phase oscillator networks. *Chaos*, 22(4):043104, 2012.

[42] Carlo R Laing. Derivation of a neural field model from a network of theta neurons. *Physical Review E*, 90(1):010901, 2014.

[43] Carlo R Laing. Numerical bifurcation theory for high-dimensional neural models. *The Journal of Mathematical Neuroscience*, 4(1):13, 2014.

[44] Carlo R Laing, William C Troy, Boris Gutkin, and G Bard Ermentrout. Multiple bumps in a neuronal model of working memory. *SIAM Journal on Applied Mathematics*, 63(1):62–97, 2002.

[45] C.R. Laing and C.C. Chow. Stationary bumps in networks of spiking neurons. *Neural Comput.*, 13(7):1473–1494, 2001.

[46] PE Latham, BJ Richmond, PG Nelson, and S Nirenberg. Intrinsic dynamics in neuronal networks. I. Theory. *Journal of Neurophysiology*, 83(2):808–827, 2000.

[47] Timothy J Lewis and John Rinzel. Dynamics of spiking neurons connected by both inhibitory and electrical coupling. *Journal of computational neuroscience*, 14(3):283–309, 2003.

[48] Tanushree B Luke, Ernest Barreto, and Paul So. Complete classification of the macroscopic behavior of a heterogeneous network of theta neurons. *Neural computation*, 25(12):3207–3234, 2013.

[49] Seth A. Marvel and Steven H. Strogatz. Invariant submanifold for series arrays of Josephson junctions. *Chaos*, 19(1):013132, 2009.

[50] Ernest Montbrió, Diego Pazó, and Alex Roxin. Macroscopic description for networks of spiking neurons. *Phys. Rev. X*, 5:021028, Jun 2015.

[51] Oleh Omel'chenko, Matthias Wolfrum, and Carlo R Laing. Partially coherent twisted states in arrays of coupled phase oscillators. *Chaos*, 24:023102, 2014.

[52] Remus Osan and Bard Ermentrout. Two dimensional synaptically generated traveling waves in a theta-neuron neural network. *Neurocomputing*, 38:789–795, 2001.

[53] Edward Ott and Thomas M. Antonsen. Low dimensional behavior of large systems of globally coupled oscillators. *Chaos*, 18(3):037113, 2008.

[54] Edward Ott and Thomas M. Antonsen. Long time evolution of phase oscillator systems. *Chaos*, 19(2):023117, 2009.

[55] MR Owen, CR Laing, and Stephen Coombes. Bumps and rings in a two-dimensional neural field: splitting and rotational instabilities. *New Journal of Physics*, 9(10):378, 2007.

[56] Benjamin Pfeuty, Germán Mato, David Golomb, and David Hansel. Electrical synapses and synchrony: The role of intrinsic currents. *The Journal of Neuroscience*, 23(15):6280–6294, 2003.

[57] David J Pinto and G Bard Ermentrout. Spatially structured activity in synaptically coupled neuronal networks: I. Traveling fronts and pulses. *SIAM journal on Applied Mathematics*, 62(1):206–225, 2001.

[58] David J Pinto and G Bard Ermentrout. Spatially structured activity in synaptically coupled neuronal networks: II. Lateral inhibition and standing pulses. *SIAM Journal on Applied Mathematics*, 62(1):226–243, 2001.

[59] James Rankin, Daniele Avitabile, Javier Baladron, Gregory Faye, and David JB Lloyd. Continuation of localized coherent structures in nonlocal neural field equations. *SIAM Journal on Scientific Computing*, 36(1):B70–B93, 2014.

[60] Arthur Sherman and John Rinzel. Rhythmogenic effects of weak electrotonic coupling in neuronal models. *Proceedings of the National Academy of Sciences*, 89(6):2471–2474, 1992.

[61] Paul So, Tanushree B Luke, and Ernest Barreto. Networks of theta neurons with time-varying excitability: Macroscopic chaos, multistability, and final-state uncertainty. *Physica D: Nonlinear Phenomena*, 267:16–26, 2014.

[62] Moira L Steyn-Ross, D Alistair Steyn-Ross, James W Sleigh, and David Robin Whiting. Theoretical predictions for spatial covariance of the electroencephalographic signal during the anesthetic-induced phase transition: Increased correlation length and emergence of spatial self-organization. *Physical Review E*, 68(2):021902, 2003.

[63] Moira L Steyn-Ross, D Alistair Steyn-Ross, Marcus T Wilson, and James W Sleigh. Gap junctions mediate large-scale turing structures in a mean-field cortex driven by subcortical noise. *Physical Review E*, 76(1):011916, 2007.

[64] S.H. Strogatz. From Kuramoto to Crawford: exploring the onset of synchronization in populations of coupled oscillators. *Physica D*, 143(1-4):1–20, 2000.

[65] Klaus Wimmer, Duane Q Nykamp, Christos Constantinidis, and Albert Compte. Bump attractor dynamics in prefrontal cortex explains behavioral precision in spatial working memory. *Nature neuroscience*, 2014.

[66] Kechen Zhang. Representation of spatial orientation by the intrinsic dynamics of the head-direction cell ensemble: a theory. *The journal of neuroscience*, 16(6):2112–2126, 1996.

E-mail address: c.r.laing@massey.ac.nz

Institute of Natural and Mathematical Sciences, Massey University, Private Bag 102-904 NSMC, Auckland, New Zealand., phone: +64-9-414 0800 extn. 43512 fax: +64-9-4418136